Hot Forging Tool Design for a Magnesium Alloy Front Lower Control Arm

by

Tharindu A. Kodippili

A thesis
presented to the University of Waterloo
in fulfillment of the
thesis requirement for the degree of
Masters of Applied Science
in
Mechanical Engineering

Waterloo, Ontario, Canada, 2018

Author's Declaration

I hereby declare that I am the sole author of this thesis. This is a true copy of the thesis, including any required final revisions, as accepted by my examiners.

I understand that my thesis may be made electronically available to the public.

Tharindu A. Kodippili

Abstract

In an effort to improve fuel economy standards in the automotive industry, the use of lightweight materials to manufacture fatigue-critical components is investigated by a large group at the University of Waterloo. Prior research into the development of a front lower control arm made of a magnesium alloy has produced a design approximately 35% lighter in mass to its cast aluminum benchmark. A hot forging tool was designed and developed to produce forgings of this control arm design in a single-hit operation. The as-forged component has a shape of a near-complete arm with excess flash, requiring subsequent trimming and finishing operations. The tool was designed for a low-volume production rate and batch size – tool wear was neglected – at a maximum operational temperature of 400°C and a loading capacity of 1600 tonnes. The tool design was successfully validated using thermal and mechanical simulations. Forging materials and conditions were initially chosen based on literature. At a later time, an analytical material selection model or objective function was developed by other members involved in the project. As part of a secondary study, the structural and fatigue behaviour of the control arm forged at conditions selected using the analytical model were evaluated to gauge its effectiveness as a selection tool. Results were inconclusive due to lack of complete material models. However, through simulation, it was shown that a control arm forged at 250℃ using an extruded AZ80 alloy will meet OEM performance requirements.

Acknowledgements

Foremost, I would like to express my sincere gratitude to my advisor, Dr. Steve Lambert for providing me with the opportunity to work on this project. I would like to thank Dr. Lambert and Dr. Mary Wells for their guidance and support throughout the development of the forging tool. Also, I would like to thank my research partner, Talal Paracha for supporting me with my research activities.

I am thankful to Andrew Gryguc, Dwayne Toscano and Ali Karparvarfard and my fellow APC project researchers for helping me form the ideas and results presented in this documents.

I would also like to thank Alex Duquette, Tom Sparrow, Jim Prsa, Oleg Udarchik and Hendrik Zwaan from Multimatic, and Jonathan McKinley from CanmetMATERIALS, for without their help, the design and development of the forging tool would not have been possible.

Lastly, I would like to sincerely thank my parents for their encouragement and support throughout the course of this project.

Table of Contents

Author's Declaration ii
Abstract iii
Acknowledgements iv
List of Figures vii
List of Tables x
Chapter 1 Introduction 1
1.1 Motivation 1
1.2 Objectives 2
1.3 Thesis Overview 4
Chapter 2 Background and Literature Review 5
2.1 Magnesium Alloys 5
2.2 Forging 6
2.2.1 Forging Process 7
2.2.2 Closed-Die Forging 8
2.2.3 Classification of Forging Machines 10
2.3 Forming Tool Design Principals 11
2.3.1 Forged Material 12
2.3.2 Die Block Geometry and Material 14
2.3.3 Parting Line 15
2.3.4 Die Side Thrust 16
2.3.5 Corner Radii 17
2.3.6 Fillet Radii 17
2.3.7 Ribs and Webs 19
2.3.8 Draft Angles 21
2.3.9 Flash and Gutter 21
2.4 Forging Tool Components 22
2.5 Modes of Die Failure 24
2.6 Forging Simulations 25
2.7 Preform Design 26
Chapter 3 Forging Tool Assembly Design 28
3.1 Design Overview 28

3.1.1 Design Specifications 29
3.2 First Conceptual Design 31
3.2.1 Lower Forming Tool Design 32
3.2.2 Heater Plate 35
3.2.3 Insulation 38
3.2.4 Support Pucks 38
3.2.5 Platen 39
3.3 Second Conceptual Design 39
3.3.1 Upper and Lower Forming Tools 41
3.3.2 Upper and Lower Heel Blocks 42
3.3.3 Second Heater Plate Design 44
3.3.4 Second Platen Design 44
3.4 Third Conceptual Design 46
3.4.1 Upper and Lower Forming Tools 47
3.4.2 Second Support Puck Design 48
Chapter 4 Detail Design and Verification 49
4.1 Detailed Design Geometry 49
4.2 Thermal Analysis 52
4.3 Structural Analysis 56
Chapter 5 Control Arm Performance Analyses 62
5.1.1 Finite Element Model 63
5.1.2 Finite Element Model Setup Validation 65
5.1.3 Strength Analysis Results 68
5.1.4 Fatigue Life Analysis Results 70
Chapter 6 Conclusions and Recommendations 74
6.1 Conclusions 74
6.2 Recommendations 75
References 77
Appendix A Analytical Calculations 81

List of Figures

Figure 1: Ford Baseline LH Control Arm Design 3
Figure 2: Grain structure in forging, bar stock, and casting [4] 5
Figure 3: Forging process design flow chart (modified from [11]) 7
Figure 4: Fully closed die configuration. Flash width (b). Flash gap (s) [12] 8
Figure 5: 1200-Tonne hydraulic press at CanmetMATERIALS [17] 11
Figure 6: Undesirable – Parting line locations resulting in metal flow patterns that cause potential forging defects [4] 15
Figure 7: Desirable – flow patterns are smooth at stressed sections given the location of parting lines [4] 16
Figure 8: Desirable – parting line outside a rib or wall follow the web inside the forging [4] 16
Figure 9: Preferred – inclined forging with respect to forging plane (right). Counterlocks (left) are expensive to build [4] 17
Figure 10: Recommended fillet radii for various sections of a forging [4] 18
Figure 11: Rib edge design comparison. (Left) flat-edged rib. (Right) recommended round-edged rib [4] 19
Figure 12: (Right) thickening at the centre of thin and wide web's. (Left) Use of punch-out holes in relieving excess metal in web sections [4] 20
Figure 13: Design features at rib and web adjoining surfaces: (right) tapered web, (left) full radius fillet [4] 20
Figure 14: Conventional flash and gutter design [4] 22
Figure 15: Anchor Danly die set. Forming tool not shown [28] 22
Figure 16: (Left) sliding ejector pin mechanism. (Right) hinged ejector pin mechanism [29] 23
Figure 17: (Right) strip heaters. (Left) heater cartridges [31] 24
Figure 18: Preform: 63.5mm dia. x 716mm extruded AZ80 bar stock with a 108º bend angle 27
Figure 19: Tool development flow chart 28
Figure 20: Macrodyne 1200-tonne & 1500-tonne presses at CanmetMATERIALS [17] 30
Figure 21: Exploded view of the lower forging tool showing key components (1st design iteration) .. 31
Figure 22: Section view of the deepest cavity region of the control arm geometry. (rb) rib thickness. (do) draft angle. (ri) fillet radii. 33
Figure 23: Section view of the thinnest web region of the control arm geometry. (re) corner radii. (wb) web thickness. 34

Figure 24: Impression tool - cutting surfaces. (Blue) 3.3mm thick parting line. (Green) upper impression surface. (Red) lower impression surface. 34
Figure 25: Lower forming tool (1st design iteration)..... 35
Figure 26: Isometric view of heater plate (1st design iteration) 36
Figure 27: Side view of forming tool and heater plate..... 36
Figure 28: Basic platen design 39
Figure 29: Forging tool side view cross section (2nd design iteration)..... 40
Figure 30: Forging tool second conceptual design 41
Figure 31: (Left) Upper Forming Tool. (Right) Lower Forming Tool. 42
Figure 32: (Left) lower heel block. (Right) upper heel block 43
Figure 33: Cross section view of upper and lower tool engaged 43
Figure 34: Lower Platen (2nd design iteration)..... 45
Figure 35: Upper Platen (2nd design iteration) 45
Figure 36: Forging Tool Assembly (3rd design iteration) 46
Figure 37: Puck arrangement modification..... 47
Figure 38: (Left) upper and (right) lower forming tool (3rd design iteration) 48
Figure 39: Upper forging tool (reproduced from [36]) 50
Figure 40: Lower forging tool (reproduced from [36])..... 50
Figure 41: Puck configuration is shown (reproduced from [34]) 51
Figure 42: Upper and lower tools being assembled at Multimatic Technical Centre 51
Figure 43: Temperature field over forming surface (upper tool). Heating time: 3.40 hours 53
Figure 44: Temperature field over forming surface (lower tool). Heating time: 3.75 hours 54
Figure 45: Temperature field over forming surface (upper tool) 55
Figure 46: Temperature field over forming surface (lower tool) 55
Figure 47: Deformed AZ80 preform at 400℃ **under 900 tonne peak load. Preform and forming tool** contact region is shown in green (reproduced from [10]) 57
Figure 48: Von Mises stress contours on upper forming tool surface. Max value = 201 MPa. 58
Figure 49: Von Mises stress contours on lower forming tool surface. Max value = 270 MPa. 58
Figure 50: Von Mises stress contours on lower tool support pucks 59
Figure 51: Support puck yield location (lower tool). Max value = 842 MPa. 59
Figure 52: Upper tool nodal displacement (Z-direction). Max value = 0.26 mm 60
Figure 53: Lower tool nodal displacement (Z-direction). Min value = -0.47mm 60

Figure 54: Final Control Arm Geometry 62
Figure 55: Control arm mesh. (Red) as-forged surface. (Blue) machined surface 63
Figure 56: Comparison of Magnesium Material Models [45] [46] [44] 64
Figure 57: Geometrical differences between control arm designs. (Left) 13097-0002 R006. (Right) 13097-0000-2 R009. 65
Figure 58: Tie-rod cut out region 65
Figure 59: Global-level model. Control arm connected to suspension stiffness model 66
Figure 60: Deformed component forged using AZ80 alloy at 250℃. Achieved 100% of L2 load. Component experiences a maximum strain of 2.7%. 68
Figure 61: Deformed component forged using AZ31B alloy at 250℃. Achieved 66% of L2 load. Component experiences a maximum strain of 4.0%. 69
Figure 62: Deformed component forged using ZK60 alloy at 250℃ Achieved 97% of L2 load. Component experiences a maximum strain of 3.6%. 69
Figure 63: Minimum fatigue life of FLCA forged from AZ80 alloy at 250℃. Minimum fatigue life of the component is 4.07 71
Figure 64: Minimum fatigue life of FLCA forged from AZ31B alloy at 250℃. Minimum fatigue life of the component is 1.97 71
Figure 65: Minimum fatigue life of FLCA forged from ZK60 alloy at 250℃. Minimum fatigue life of the component is 3.81 72

List of Tables

Table 1: ISO 2768-mk tolerances assigned to component 9
Table 2: Objective function values (reproduced [20]) 14
Table 3: Die machining methods and achievable accuracy [23] 14
Table 4: CanmetMATERIALS-Forging press dimensions. (BH - Blank Holder, PH – Punch Holder) [17] 30
Table 5: Geometric Specifications (reproduced from [6]) 33
Table 6: Heater Cartridge Specifications 37
Table 7: Heater cartridge duty cycle 54
Table 8: Material Properties 57
Table 9 : Model Information 63
Table 10: Equivalent plastic strain of material (reproduced from [6]) 64
Table 11: Percentage difference between Author's and Prsa's control arm simulation results (Adapted from [9]) 67
Table 12: Tabulated strength and fatigue analysis results. Objective function score, φ, provided for each material forging condition 72

Chapter 1
Introduction

1.1 Motivation

Throughout the course of the past decade, the automotive sector has been steadily incorporating lightweight materials to manufacture structural automotive components in an effort to meet new environmental regulatory targets on fuel consumption and greenhouse gas emissions [1]. Incorporating lightweight materials in the vehicle reduces the gross vehicle mass (GVM), which in turn reduces the performance requirements of the engine, suspension and brake system [2]. A 10% reduction in vehicle mass will result in approximately 5.7% - 7.4% reduction in fuel consumption [1]. In addition, weight reductions made to the unsprung mass directly improves the vehicle handling and ride performance, improving vehicle response and ride comfort.

Magnesium – most commonly found in the earth's ocean – and its alloys are amongst the alternative lightweight materials considered, along with high strength steel (HSS), aluminum, glass and carbon-fiber reinforcement polymer composites. Magnesium is the lightest structural metal available for commercial use. With a density of only 1.7-1.8 g/cm^3, magnesium alloys have the greatest advantage owing to its low density. Aluminum alloys in comparison have a density of 2.5 to 3.0 g/cm^3. In addition, magnesium has high specific strength and electromagnetic interference shielding capability [3]. The full potential use of this material, however, has yet to be actualized. Current applications of the material have been limited to trim and non-load bearing components such as instrument panels and steering components.

A variety of magnesium alloys have been developed for manufacturing. The most common alloys are M1A, AZ31B, AZ61A, AZ80A, and ZK60A. Typical uses of these alloys can be seen in extrusions, especially AZ31B, which is commonly used in sheet metal manufacturing [4].

Magnesium alloys are difficult to deform due to its hexagonal closed packed (HCP) crystal lattice structure. The HCP structure restricts deformation due to a limited number of slip systems that are active at lower temperatures. Magnesium alloys are well suited to replace engineering metals and plastics in many applications due to their favourable densities, higher stiffness, higher recyclability and lower production cost [5]. However, magnesium alloys are susceptible to galvanic corrosion. A common way to minimize galvanic corrosion is to reduce the chemical potential difference between alloying elements. Alloys such as AZ91E, WE43B and Elektron 21 are corrosion resistant alloys (refer to Appendix A for a

complete list of alloys and potential uses) [5]. Even though the use of alloying elements can provide significant improvement in corrosion resistance, a subsequent step involving coating is usually required, specifically in cases where the component is in contact with metals with a different chemical potential. Potential coating methods are fluoride anodizing, chemical treatments, electrolytic anodizing, sealing with epoxy resins, standard paint finishes, vitreous enameling, electroplating and cold spray [5].

Historically, die casting has been the most prevalent form of manufacturing automotive components; over 90% of automotive components are manufactured via this method [1]. The use of cast magnesium has been limited to non-loadbearing applications due to insufficiencies in the mechanical performance of the material. Forged magnesium, however, does not have this limitation and has been shown to produce superior mechanical properties, and is suitable for producing structural components [5].

The proposed research, to forge a fatigue critical automotive component from a magnesium alloy, is supported by the Automotive Partnership Canada (APC). The project teams include the University of Waterloo, Ford Motor Company, Multimatic Technical Centre (MTC), CanmetMATERIALS, and Centerline Ltd.

1.2 Objectives

The overarching goal of the APC project is the optimum design, development and validation of a light-weight magnesium automotive suspension component which is equivalent in performance and durability to a baseline cast aluminum. A front lower control arm (FLCA) from a Ford platform was chosen. The current cast aluminum FLCA weighs 2.3 kg, and a 20% reduction of component mass is targeted for the magnesium replacement [1].

Figure 1: Ford Baseline LH Control Arm Design

To achieve the APC project objectives, six project teams were assembled: design (author's group), forging, fatigue, residual stresses, corrosion and residual stress measurement. There is ongoing support from industry partners: Multimatic Technical Corporation (MTC), CanmetMATERIALS, Centreline, and Ford Motor Company. Prior to the author's involvement in the project, Alex Strong and Yu Guo carried out design related tasks. Strong was responsible for developing the preliminary magnesium control arm design in accordance with Ford specifications [6]. This design was then refined by Oleg Udarchik. The performance of the design was verified by Jim Prsa. The final control arm geometry conceived through this effort weighed 1.5 kg, achieving approximately a 35% weight reduction. Forged magnesium alloy properties used in the component simulations were produced by Yu Guo, Andrew Gryguc, Dwayne Toscano and Ali Karparvarfard, members of the design, forging and fatigue task groups.

The responsibility of the author was the design and verification of a tool capable of forging a magnesium alloy control arm at elevated temperatures. The author collaborated closely with Talal Paracha who performed material flow simulations [10] to design a suitable preform billet shape and to optimize the forming tool geometry. As a secondary task, the author conducted strength and fatigue performance analyses on the control arm using three magnesium alloys. The three alloys were ranked based on control arm performance and compared with the ranking order obtained from an analytical function developed by the Fatigue Task group to rank magnesium alloys based on their forging condition.

1.3 Thesis Overview

The present thesis is composed of five main sections:

In chapter 2, background information necessary for die design is provided. The benefits of forging, descriptions of equipment and die tools used in the forming process, magnesium alloy selection, forging process variables, process simulations to predict metal flow, tool design guidelines, preform design guidelines, and heat transfer theory are discussed.

In chapter 3, the design and development of the forging tool are discussed: design requirements, constraints and criteria, and conceptual designs are presented in detail.

Chapter 4 details the results of numerical analyses which were performed to validate the final die design. Thermal and mechanical finite element analysis were performed on the forging tool to assess the temperature field over the forming surface and heating time, and maximum load capacity.

In chapter 5, the performance of the final control arm is evaluated using material properties of three forged materials. Based on strength and fatigue simulation results, a score is assigned to the forged material validating its use for forming the control arm. Scores are presented alongside material rankings which were derived analytically using an objective function developed by the fatigue task group.

Chapter 6 presents the conclusions and recommendations.

Chapter 2
Background and Literature Review

Forging is a metal working process that involves the shaping of a work piece by compression within two dies. By means of forging, components with higher strength, toughness and reliability can be produced. Forging offers an advantage over other metal working techniques due to the increased degree of material deformation control during the forging process. By controlling the directional alignment of material, or grain flow, directional properties such as strength, ductility and resistance to fatigue can be potentially improved. Forged components, therefore, have superior characteristics relative to components produced via alternate forms of metal working. The process is capable of producing high quality parts at a moderate cost [4].

2.1 Magnesium Alloys

During a forging operation, grain flow closely follows the impression tool outlines producing a more continuous grain flow in comparison to components machined from bar stock or produced through casting operations. Machined components exhibit a unidirectional grain flow; machined or sheared segments of the stock exhibit sharp directional changes in the flow lines, exposing grain ends. This renders machined components more susceptible to fatigue and more sensitive to stress corrosion cracking [4]. Components made from casting have no grain flow and have worse material characteristics. In comparison to welded components, forgings are also superior. Welds are seldom free of porosity or metallurgical notches, which reduce the fatigue life of a component. Figure 2 depicts the grain flow patterns that can be observed in a forging, bar stock, and casting.

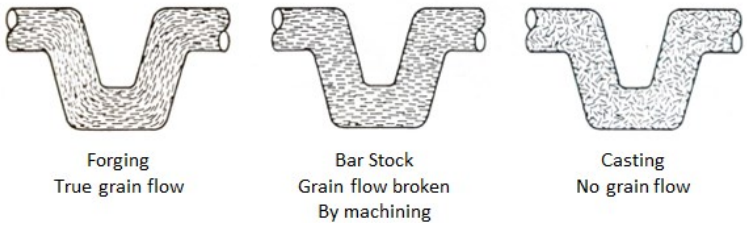

Figure 2: Grain structure in forging, bar stock, and casting [4]

Forging provides an improved degree of structural reliability by eliminating gas pockets and voids which could cause unexpected failure under stress or impact. A superior chemical uniformity can also be achieved through the dispersion of alloy during die filling. The uniformity in composition that can be achieved through forging ensures consistency of material properties from one component to the next, and a reproducible response to post-processing heat treatment operations, and minimal variation in machinability. Forging surfaces also provide a dependable surface for metal cutting processes such as turning, milling, drilling, boring, broaching, shaping process etc. In addition, these components are well suited for welding as the near absence of internal defects and the inherent fine-grain structure of the forging provide an optimal welding surface [4].

2.2 Forging

The forging process design used in this research project was acquired from literature [11] and modified. Initially, the functional requirements of the forged component are established, followed by a topology and shape optimization process to derive the final part geometry and the as-forged geometry. In the subsequent process selection step, the forging material, forging equipment, quantity of parts expected to forged, and the overall economy of the process are established. Then, a preliminary die design is conceived; tool impression is created using the as-forged geometry of the component. During this stage, material flow simulations are conducted to verify the forging operation along with die design modifications. Upon completion of this iterative process, a final die design is produced and subjected to thermal and mechanical analyses. Once tool performance is verified, a CAD package is created for tool fabrication, followed by installation in the press. The flow diagram illustrated in Figure 3, highlights the steps involved in the forging design process.

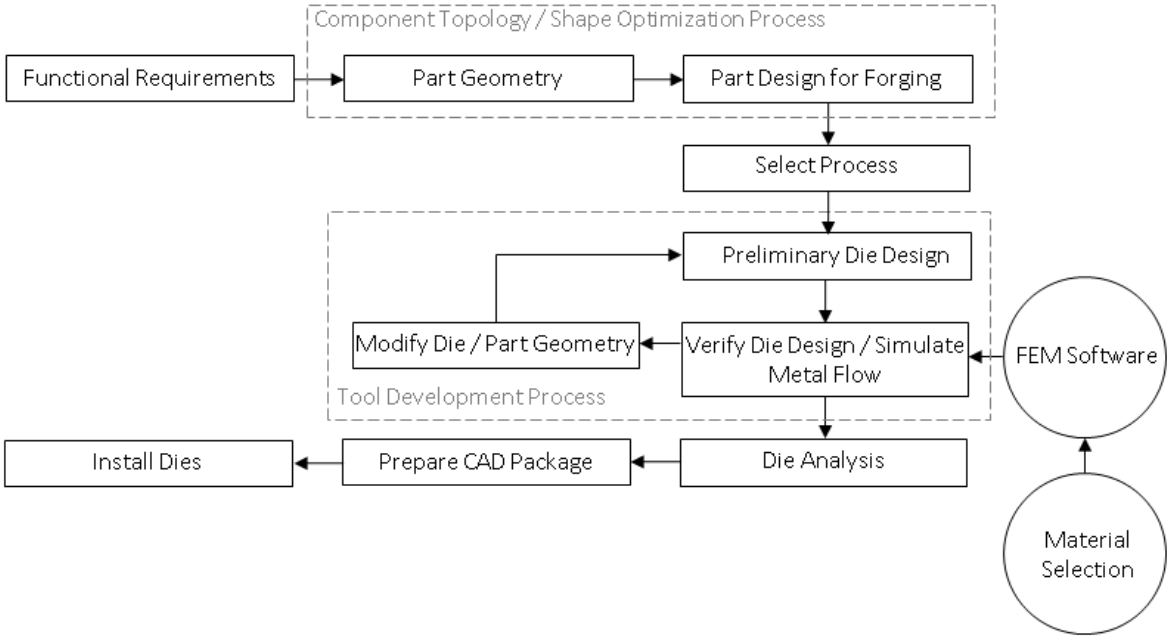

Figure 3: Forging process design flow chart (modified from [11])

2.2.1 Forging Process

The forging process can be categorized into either a multi-step or single-step, open-die or closed-die forging. Open-die forging does not confine the metal laterally when it is being compressed axially by the upper and lower die tool into the desired shape. The process involves the use of a standard flat, V-shaped, concave, or convex die for deformation of the work piece, allowing for grain flow in either one or two directions. During open-die forging, the work piece is often repeatedly hammered by a mechanical or hydraulic press to progressively work the piece into the desired shape [4]. Components with simple shapes such as shafts, ring-like parts, and contour formed metal shells can be produced through open-die forging.

During closed-die forging, also known as impression forging, the work piece is shaped between closed die cavities via forging presses or hammers. Mechanical presses and hydraulic presses, each possessing unique advantages, are the primary equipment used. As the ram forces the impression tools together, the work piece deforms plastically and metal flows laterally within the impression cavity; dispersion of material is bounded by the impression wall. Any excess metal, commonly referred to as flash, is forced

outward from the impression through what is known as the flash land into a cavity referred to as the gutter. Allowing for the excess metal to accumulate into this space facilitates die closure and enables the die mating surfaces to touch. The desired dimensional accuracy is ensured when the die is in the fully closed configuration as shown in Figure 4. Having the flash forced out of the impression leads to the development of high die stresses in the surrounding flash area. This constraining of the material leads to improved material properties in the final part, but also reduces tool life and requires higher press loads for deforming the material. These critical factors have to be taken into consideration when designing a closed-die forging tool. Closed-die forging make possible forging of more complex shapes, and was used in the current project.

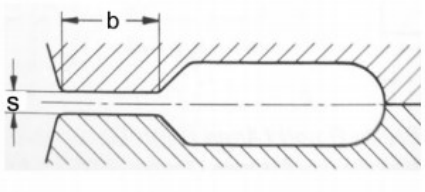

Figure 4: Fully closed die configuration. Flash width (b). Flash gap (s) [12]

2.2.2 Closed-Die Forging

The closed-die forging process can be categorized according to the temperature at which the operation is carried out. The process can be identified as either a hot, warm or cold forging operation. Forgeability of a work piece – the relative ability of a material to deform without rupture – is directly influenced by the temperature at which the operation is performed.

Typically, cold forging operations are carried out at room temperature. The main advantage of such an operation is in the material savings that can be made by forging precision shapes requiring minimal machining and finishing attributing to lower thermal contraction effects and less flash. Cost of die tooling is usually higher however, as tooling requires a higher degree of structural integrity to withstand the larger forging loads. It is possible to achieve overall dimensional tolerances ranging from IT7-IT11 of ISO IT standards [13] with cold forging. Component dimensional tolerances are specified to ISO 2768-

mk standards; linear and position tolerances are provided in Table 1. Due to poor formability of magnesium at low temperatures, cold forging is not considered.

Warm forging operations are performed at temperatures above the work-hardening temperature of the material, and below scale formation temperatures. For magnesium alloys, this involves forming at temperatures below 300℃ [14]. Advantages of warm forging can be observed in the reduced load required to forge the component relative to cold-forging. Also, favorable as-forged properties of the component can potentially serve to eliminate subsequent heat treatment processes. Tolerances ranging from IT9-IT12 of ISO IT standards can be achieved [13] with warm forging. Additional slip systems become active at around 225℃ for magnesium alloys [15], so warm forming is an option. A disadvantage of warm-forging can be attributed to the added economical cost from the inclusion of a controllable heating system [15].

Hot forging operations are carried out at a temperature above the recrystallization temperature of the work piece, avoiding strain hardening. The benefits in a hot forging operation can be seen in the degree of work piece deformation during a single operation in comparison to the other two processes. As a result, die wear can be reduced. Disadvantages may arise from scale formation at elevated temperatures, and lower dimensional accuracy resulting from thermal contraction. Tolerances of ranging from IT12-IT16 of ISO IT standards can be achieved [13]. Similarly to warm-forging, the work-piece is pre-heated and placed between separated dies during the press-open interval of the forming cycle. Dies are internally heated and the work-piece is forged into the desired shape during the press-close interval. The forged component is then ejected, cooled and subjected to trimming and machining operations.

Table 1: ISO 2768-mk tolerances assigned to component

	Linear dimension (mm) [over 120 up to 400]	External radius & chamfer heights (mm) [over 3 up to 6]	Straightness and flatness (mm) [over 100 up to 300]
Permissible deviations in nominal length (mm)	+/- 0.5	+/- 0.5	0.4

Forging the component via a cold-forging operation was not considered due to the poor formability of the material at ambient temperatures. A hot forging tool capable of forging above 300℃ is suitable, owing to the possibility of forging over a wider range of temperatures.

2.2.3 Classification of Forging Machines

A variety of machines can be used during the forging process. These include hammer forging machines (Board Drop Hammers, Power Drop, Counter Drop and Air-lift Gravity Drop Hammers), press forging machines (mechanical press, hydraulic press and screw press), and horizontal and roll forging machines [16].

Hammer forging machines, with the exception of counterblow hammers, have a weighted ram which moves vertically in a downward stroke exerting a striking force on a heated work piece. They are classified as energy-restricted machines. The upper die tool is fastened onto the weighted ram, and the lower die tool to the anvil near the base of the hammer. The kinetic energy of the weight ram is imparted into the work piece by dealing heavy and quick blows. It is dissipated by plastically deforming the work piece and by elastically deforming the ram and die tool. The remaining energy is dissipated in the form of heat [4].

Press forging machines are further classified into either hydraulic or mechanical press forging machines. They are more commonly used in close-die forging since slow and continuous pressures can be applied on the work-piece. The ram in most mechanical presses is actuated via a slider-crank mechanism which translates rotary motion into reciprocating linear motion, causing the ram and die tool to press and deform the work piece. A hydraulic press uses hydraulic pistons to press on the work, typically with a uniform load throughout the entire duration of the stroke. Hydraulic presses deliver load control or ram speed control during the stroke cycle, which enables the machines to forge certain alloys that would otherwise break under the blows of a hammer machine [4] [16]. CanmetMATERIALS has fully instrumented hydraulic forging presses with 110 Tonne, 1200 Tonne (Figure 5), and 1500 Tonne capacity. Access to these machines facilitated forging trials which were previously conducted to obtain material properties of forged magnesium and developing manufacturing design specifications [7]. Forging operations at CanmetMATERIALS were carried out by Lucian Blaga, under the direction of Bruce Williams and Joathan McKinley [10] [7].

Figure 5: 1200-Tonne hydraulic press at CanmetMATERIALS [17]

2.3 Forming Tool Design Principals

The type of forming tool or forging die used during a forging operation can be classified into four types: blocker-type, finish-type, conventional or precision forging type.

Blocker-type forging dies are designed with large fillets and corner radii, thick webs and ribs. Forgings made using a blocker-type die typically require a subsequent machining or finishing step. Blocker-type dies are typically used when the quantity of required parts are limited. To produce forgings using this type of die, press equipment must be capable of applying a unit pressure of 130 to 200 MPa of project plan area depending on the material and complexity of design [4].

A conventional forging die is the most commonly used in production. It is similar to a blocker-type die, but contains sharper details and is expected to produce components with tighter tolerances. As expected, forgings are more difficult to forge. A typical unit pressure of 200 to 350 MPa of plan area is required [4].

Finish-only forging dies are similar to a conventional die type with the difference being decreased fillet radii and die closure tolerances. A typical unit pressure of 200 to 350 Mpa of plan area is required [4].

Precision forging, as the name implies are used to produce forgings with the sharpest details and closest tolerances. Equipment must typically be capable of applying pressure between the ranges of 275 to 480

MPa, and the work piece is usually subjected to a blocking operation prior to undergoing the finishing operation [4] [18].

Since only a limited number of components are needed to be forged as per the scope of the research project – approximately 100 parts – a single precision forging die is desired.

2.3.1 Forged Material

The mechanical properties of the material and the forging temperature directly influences the formability, surface quality and dimensional tolerance of the forged part [18]. For the purposes of developing a magnesium alloy control arm, three alloys were originally considered: AZ31B, AZ80 and ZK60. AZ31B is a medium-strength alloy which is weldable and has good formability properties. It is commonly used in the form of sheet metals; sheets of AZ31 have been used to develop prototype automotive sheet panels, but the cost associated with producing such panels are high and as such are not often seen in automotive applications [5]. AZ80 alloys exhibit high strength properties while ZK60 alloys exhibit better formability properties. ZK60 alloys are more expensive than AZ80 due to the presence of rare elements.

The University of Waterloo Fatigue Task group and Guo [7] conducted forgability studies on AZ31, ZK60 and AZ80 magnesium alloys. They examined the stress-strain relationships at various forging temperatures and strain rates, the effect of friction on forging, and the post-forging microstructure, and the monotonic and fatigue material properties [1]. The most promising material properties were obtained from extruded AZ80, forged at 250°C [19]. These post-forged material properties were then used by Strong to develop and verify a preliminary control arm geometry [6]. This was further refined by Oleg Udarchik [8] from MTC, and verified by Jim Prsa [9], also from MTC.

At a later time, a strategy to optimize the material selection based on forging conditions was developed by the University of Waterloo APC Project Fatigue Task Group. The fitness of an alloy, forged using cast or extruded billets at varying forging temperatures and a forging speed of 20mm/s was quantitatively evaluated using an objective function [20]. I-beam forging samples were used to obtain the tensile and cyclic material properties corresponding to each forging condition [7].

The objective function considers the static behaviour,φ_1 fatigue behaviour,φ_2 and hardness,φ_3 of the alloy. Weighting factors are assigned to strength, fatigue and hardness behaviours of the alloy based on engineering judgement to quantitatively express the degree of significance of each parameter in measuring the performance of the control arm [20]:

$$\Phi = 0.5\varphi_1 + 0.4\varphi_2 + 0.1\varphi_3$$

The static behaviour of a specific alloy was expressed in the form:

$$\varphi_1 = 0.5\frac{S_y^T}{S_{y,max}^T} + 0.5\frac{E^T}{E_{max}^T}$$

Where yield strength, $S_{y,max}^T$ and strain energy, E_{max}^T, were the maxima among all the considered materials forging conditions.

The fatigue behaviour was expressed in the form:

$$\varphi_2 = 0.65\frac{\sigma_f'}{\sigma_{f,max}'} + 0.35\frac{b_{max}-b}{b_{max}-b_{min}}$$

Where σ_f' and b are fatigue parameters acquired from material specific S-N curves.

Finally, the hardness was incorporated in the fitness function to account for material uniformity

$$\varphi_3 = \frac{H_{max}-H}{H_{max}-H_{min}}$$

Where H is the standard deviation of hardness throughout the cross-section.

Table 2 shows the fitness values evaluated for the AZ80, ZK60 and AZ31 Mg alloys forged at various temperatures. The performance of the material was ranked from 0 to 1. As illustrated in Table 2, a control arm forged at 250 °C from an extruded AZ80 alloy shows the highest fitness value of 0.84. Chapter 5 of this thesis explores the strength and fatigue performances of the component using three materials; the study was limited to three materials as material cyclic properties were unavailable for the remaining forging conditions.

Table 2: Objective function values (reproduced [20])

Alloy	Temperature °C	φ
AZ31 Cast + Forged	275	0.509
	375	0.511
AZ31 Extruded + Forged	250	0.698
	375	0.72
ZK60 Cast + Forged	250	0.623
	375	0.566
ZK60 Extruded + Forged	250	0.814
	375	0.745
AZ80 Cast + Forged	250	0.546
	275	0.466
	375	0.506
AZ80 Extruded + Forged	250	0.843
	375	0.739

2.3.2 Die Block Geometry and Material

The die block material must possess a high hardness as it is critical to the longevity of the forging tool. A well-chosen material with an appropriate hardness is essential to withstanding the strains imposed by press loads, wear, cracking, and heat checking. Materials commonly chosen for constructing forging tools used in hot forging operations are ASI H13, ASI L6 and DIEVAR steels [21]. These materials are subjected to heat treatment operations to increase the hardness to values upwards of 60 HRC or greater on the surface [22]. The tool can also be coated to increase wear resistance. Table 3 [23] shows the achievable dimensional accuracy and surface roughness of potential die machining methods. A study exploring the relationship between material flow and surface roughness in an aluminum hot forging application concluded that die roughness dominates overall effects on material flow [24].

Table 3: Die machining methods and achievable accuracy [23]

Process	Dimensional accuracy (μm)	Surface roughness (μm)
Cold hobbing	10	<5
Hot hobbing	50	<15
Turning	10	<12
Milling	200	<15
EDM	5	<5

2.3.3 Parting Line

The parting line is the separation between the upper and lower tools in a closed die set. It usually separates the top and bottom halves of the component through its maximum periphery. During forging, in addition to filling the die cavity, material is allowed to exit the die cavity along the parting line, creating flash. The parting line directly influences the initial cost of the die set and plays a considerable role in determining the wear on the die set, grain flow, ease of forging, and the mechanical properties of the forged component. It is generally placed in one plane; however, it is not uncommon to see irregular parting lines depending on the specific part geometry. The parting line must be design to ensure that the part can be removed from the die. Metal flow lines displayed in Figure 6 are undesirable as the grain flow is not smooth, and location of the parting line also has the potential to promote under-filling. Figure 7 shows desirable grain flow promoted from locating the parting line at the end of the component rib feature. As shown in Figure 8, it is desirable to have the parting line follow the centre line in a forging contain a web of varying planes enclosed by ribs. It is also recommended in the literature that a parting line does not incline more than 75°, as ragged trimmed edges may result as a consequence [4].

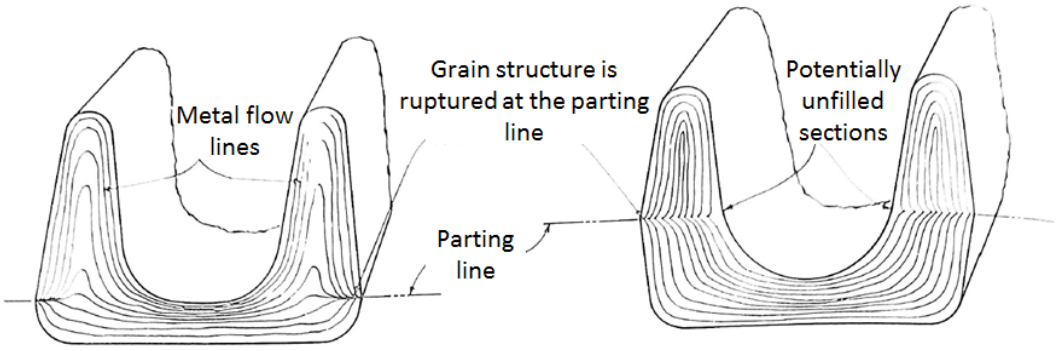

Figure 6: Undesirable – Parting line locations resulting in metal flow patterns that cause potential forging defects [4]

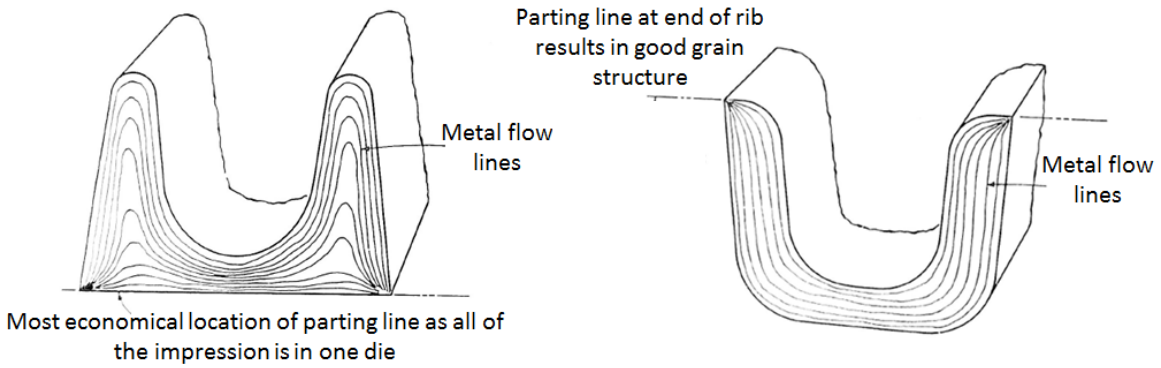

Figure 7: Desirable – flow patterns are smooth at stressed sections given the location of parting lines [4]

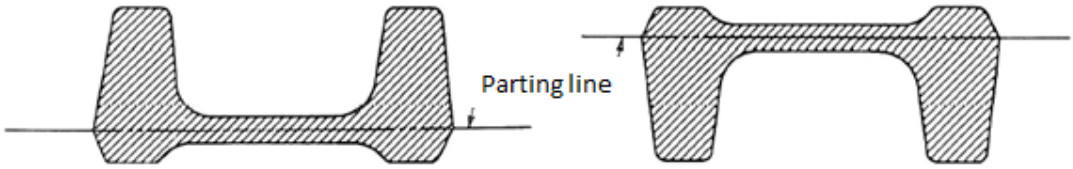

Figure 8: Desirable – parting line outside a rib or wall follow the web inside the forging [4]

2.3.4 Die Side Thrust

Die side thrust is induced in die sets with irregular (sloped) parting lines. As the parting line inclines from parallel to the forging plane, lateral loads cause the two die halves to shift and misalign. A counter lock feature, as seen in Figure 9, can be added to the die set to prevent the lateral shift, or the forging can be rotated in the die to balance the loads. Application of press load on the die set where the loads are balanced further minimizes die side thrust and the costs associated with machining members that restrain the dies [4] [25].

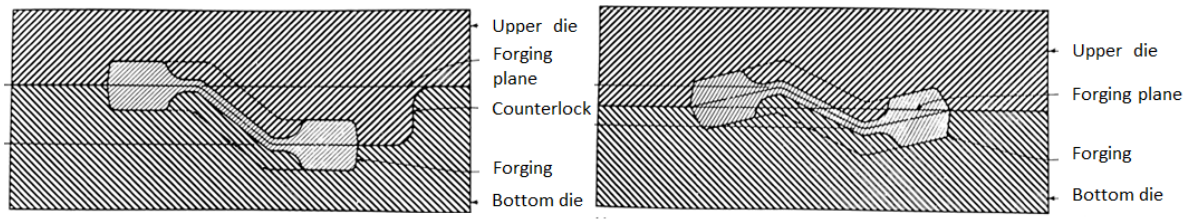

Figure 9: Preferred – inclined forging with respect to forging plane (right). Counterlocks (left) are expensive to build [4]

2.3.5 Corner Radii

A corner radius is required at the intersection of two surfaces. A forging's corner radius is formed by a corresponding fillet radius. Designing a forging to have appropriate corner radii is crucial as stress concentrations develop at these locations, both in the forging and the forging die. When a die fillet radius is excessively sharp, the metal under pressure and the corner stresses can lead to checking – a crack in the die impression – as greater pressures are required to force the metal to flow into tight corners. Using appropriate corner radii also limits the use of thin, high ribs. Based on the literature, corner radii specific to the forming tool should be greater than 2.3 mm. This was proven suitable in the present research program during I-Beam forging trials [10] [7].

2.3.6 Fillet Radii

A fillet radius within a forging is used at the intersection of two surfaces. To ensure good quality and formability, regardless of the forging type, the die design should have generous fillet radii. This allows for the metal to follow the contours of the impression during the deformation process. Small fillets can cause voids beyond the bend in the flow path of the metal, and although they may be subsequently filled, internal flaws caused by interrupted flows may occur [4]. It is recommended that when the flow of metal into the die gutter at the parting line is confined, or if the forging stock is to fill ribs on the outside periphery, large fillet radii be used. Fillet radii should blend tangent to connecting surfaces. Minimum

fillet radii of the control arm die should be greater than 10 mm; proven suitable during I-Beam forging trials [6] [7].

At intersections where the angle between the adjoining surfaces are less than 90° and with rib heights of 25 mm. or more, larger fillet radii are recommended to prevent forging flaws [4]. Section C-C as shown in Figure 10, suggests a doubling of the fillet radius in the forging section. Section A-A in Figure 10 depicts the basic shape for a straight section. If the web is enclosed by ribs and either one or both features are excessively thin, and if the width between ribs is greater than 10 times the rib height, larger than normal fillets are recommended to prevent "flow-through" effects [4]. The inadequacy of the fillet radius causes metal to flow through into the gutter without filling the rib cavity.

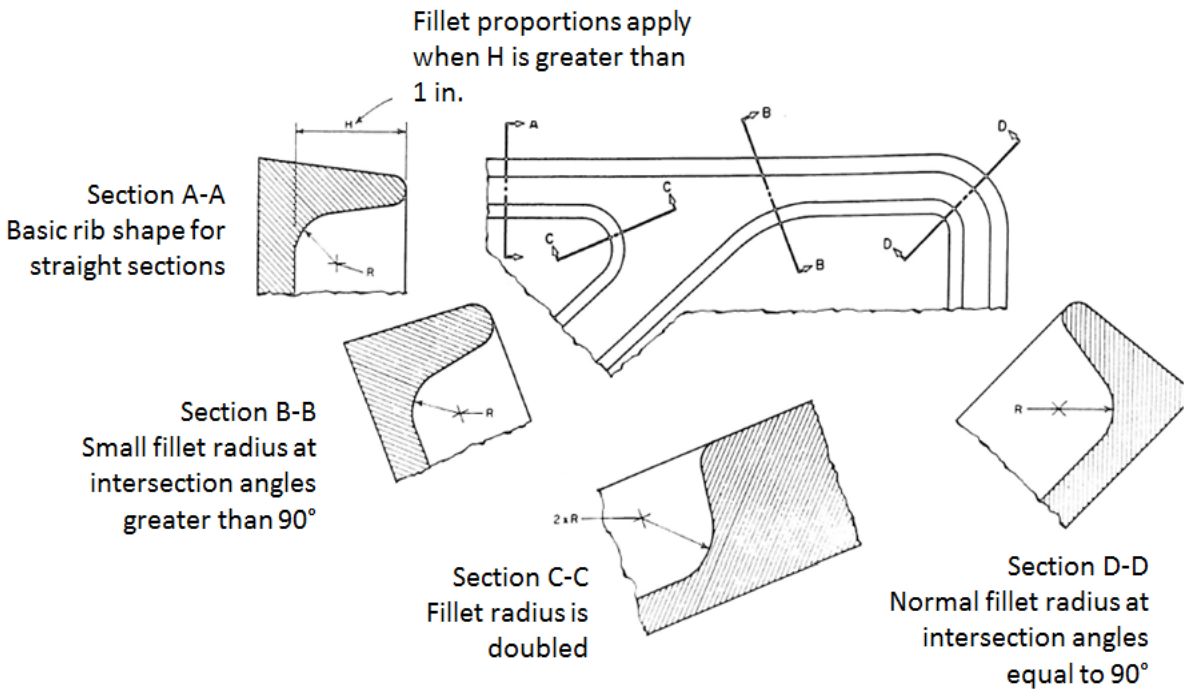

Figure 10: Recommended fillet radii for various sections of a forging [4]

2.3.7 Ribs and Webs

To maximize the life of the die, rib edges should be rounded with a full radius as shown in Figure 11. Deep, thin ribs should also be avoided when possible, particularly when adjacent to a web; excessive pressure is required to force metal into the cavity. Rib cavities next to thin webs should be made as low as possible [4].

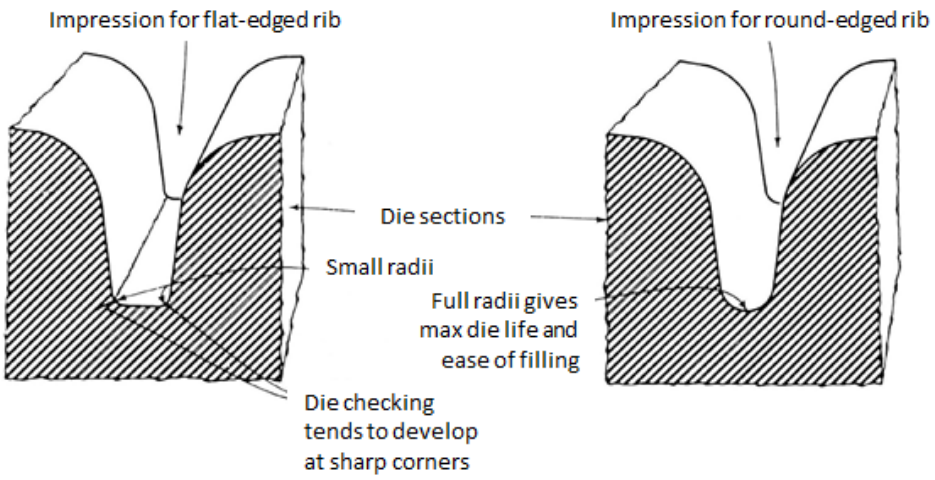

Figure 11: Rib edge design comparison. (Left) flat-edged rib. (Right) recommended round-edged rib [4]

Designing forgings with appropriate web thicknesses are important to prevent warping of web sections. Thin webs and ribs should be avoided to prevent faster cooling and shrinkage of the section in relation to the rest of the forging. Otherwise, unwanted issues such as die checking, unfilled sections and flow-through can occur. Forging excessively thin webs can impact the die tool; permanent die deflection may ensue, resulting in a thicker, middle web section, as shown in Figure 12.

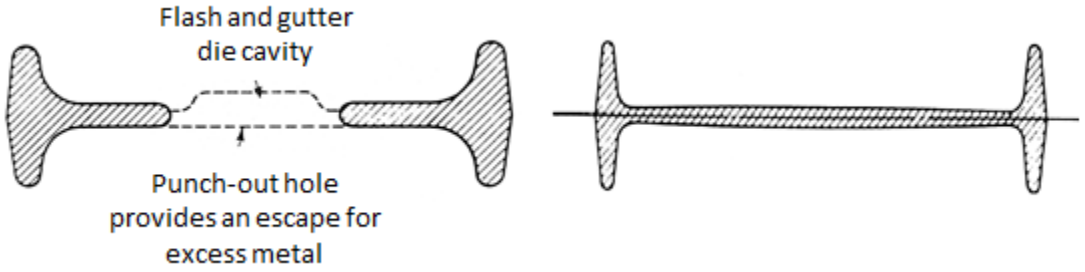

Figure 12: (Right) thickening at the centre of thin and wide web's. (Left) Use of punch-out holes in relieving excess metal in web sections [4]

Difficulty in forging webs can be reduced with the use of features such as full radii at the adjoining rib and web sections, as well as incorporating web tapers at these sections, as shown in Figure 13. An alternative to this is to incorporate punch-out holes in the forging design to minimize the total projected plan area, and consequently the pressure required to make the forging. Punch-out features are also used in areas where metal flow resistance is at its greatest. Punch-out holes allow excess metal to flow into an internal gutter [4]. I-beam forging in the current research program [7] validated the use of a minimum web thickness of 5.0 mm and a rib thickness greater than 6.35 mm.

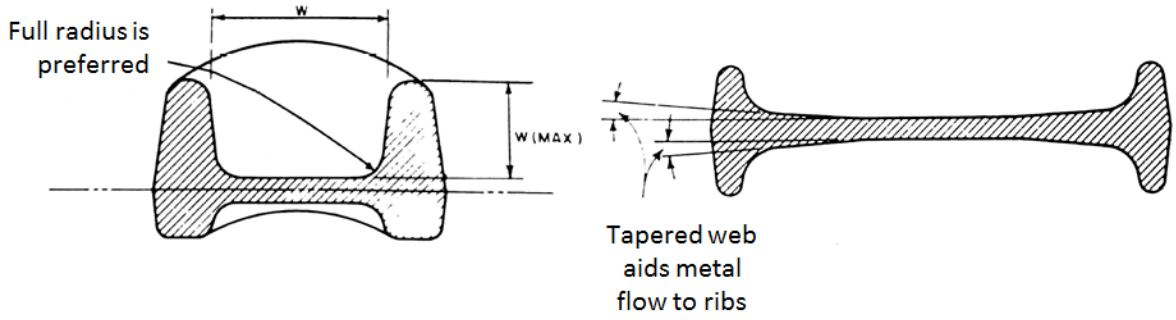

Figure 13: Design features at rib and web adjoining surfaces: (right) tapered web, (left) full radius fillet [4]

2.3.8 Draft Angles

Forgings are made with the internal and external walls at an angle from the direction of ram travel – perpendicular to the forging plane. This angle, referred to as the draft angle, is a design feature incorporated in forgings to facilitate the removal of the component from the die cavity. Common draft angles used during die sinking – the process of machining the impression into the die block – are 1°, 3°, 5°, 7°, and 10°. Removing the forging from the die with draft angles less than 5° require aids such as ejector pins; the I-beam forging dies consisted of vertical surface draft angles equivalent to 5° [6].

2.3.9 Flash and Gutter

Closed-die forging designs include a gutter or cavity for the flash – excess metal formed after the metal fills the impression cavity. The flash extends out from the body of the forging in the form of a thin extrusion around the parting line. Properly designing the flash land and the gutter is essential (Figure 14). These variables influence the quality of the forged part, forging load and die life. The flash land width and flash thickness directly influence the forging load. The forging load increases with decreasing flash thickness, and with an increase in flash land width. Appropriately chosen flash thickness and flash land width will minimize the required forging energy, and the flash allowance, the amount of excess material required in the billet to ensure that the part itself is fully formed. Sufficient frictional forces are required to restrict the flow of flash into the gutter allowing for a complete filling of the impression cavity. A volumetric approach to determining flash thickness and width shown below was used in the initial tool design [26]. During I-beam forging tool design, Guo used different flash designing guidelines to determine flash thickness and width based on weight; similar results are produced in comparison to the volumetric approach to determining flash width and thickness.

Flash thickness:

$$T_f = 1.13 + 0.0789\, V^{0.5} - 0.000134\, V\ (mm)$$

Flash land ratio:

$$\frac{W_f}{T_f} = 3 + 1.2e^{-0.00857\, V}\ (mm)$$

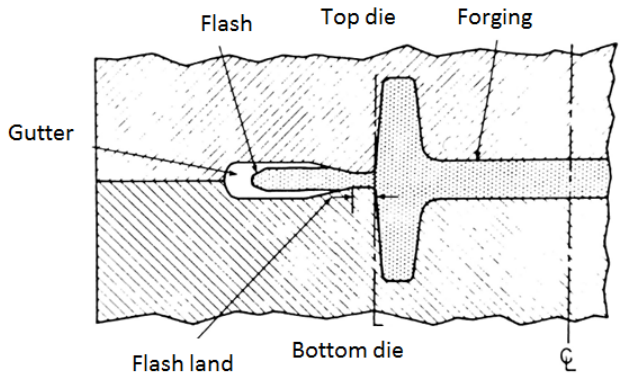

Figure 14: Conventional flash and gutter design [4]

2.4 Forging Tool Components

A forging tool is comprised of the following components [27]:

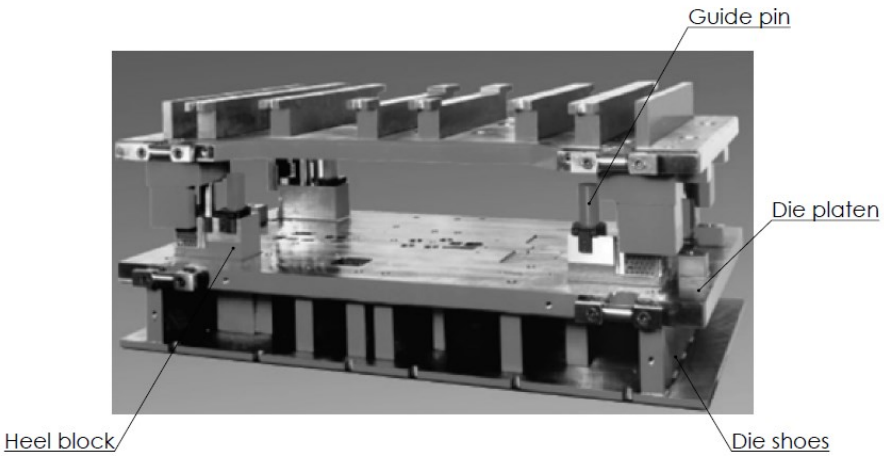

Figure 15: Anchor Danly die set. Forming tool not shown [28]

- A metal block containing the component impression cavity referred to as an impression tool, forming tool or die.
- Die platens and shoes (die set) serve as the foundation for mounting the forming tool. Figure 15 shows a pre-built Anchor Danly die set (die platen is welded to the die shoes or parallels)

- Guide pins and bushings align the upper and lower die shoes as the upper and lower die sets come together, facilitating faster production cycle times.
- Heel blocks serve the function of absorbing side thrust, as well as aligning upper and lower die sets.
- Screws dowels, spools, shoulder bolts and keepers, and keys are used to fasten and secure working components of the upper and lower die sets
- Ejector pins facilitate the release of forgings from the dies immediately after deformation. They are used to handle forgings that have been designed with less than ideal draft angles. Figure 16 shows two types of ejector pin mechanisms [ref].

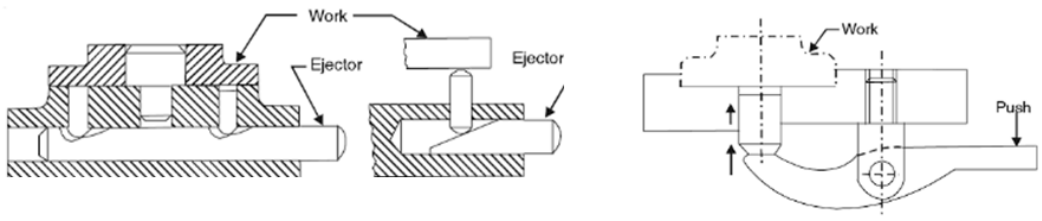

Figure 16: (Left) sliding ejector pin mechanism. (Right) hinged ejector pin mechanism [29]

Additional components such as electric heaters, thermocouples and insulation are incorporated when developing a hot forging tool. As shown in Figure 17, strip heaters are external heating elements which would be fastened on the outer periphery of the forging tool. Internal heating elements like heater cartridges are embedded inside the forging tool in order to raise the tool temperature. Only electric heating elements were considered as they prove superior to gas heaters for this particular application. Electric heating elements are relatively inexpensive, can help maintain an even and consistent die temperature over die surfaces, minimizing unwanted thermal gradients which may lead to die heat checking. Electric heating also prevents carbon deposition on die surfaces compared to gas heating; noise and explosion hazard conditions can also be avoided [30]. The use of heater cartridges over strip heaters was recommended by McKinley from CanmetMATERIALS as similar heating elements were used previously in the facility [17]. Heating elements are connected to an electrical power source, and can be externally controlled. Temperature data is collected from a thermocouple and is used to manage the power output to the heater. Form tool surface temperature is adjusted by controlling the power to each heating zone.

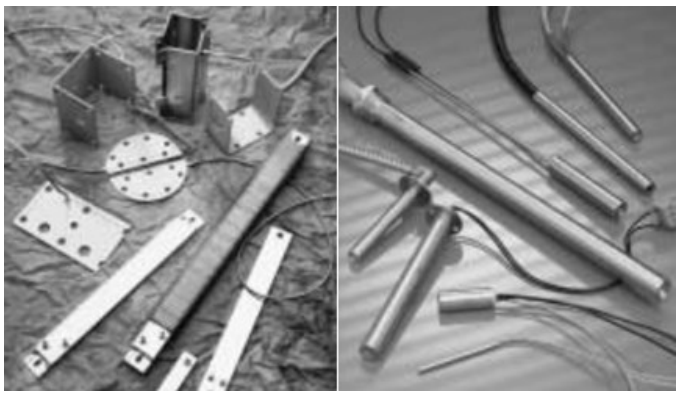

Figure 17: (Right) strip heaters. (Left) heater cartridges [31]

Heater cartridges were used in the I-beam forging tool to successfully heat the dies to ensure isothermal forging [7].

2.5 Modes of Die Failure

Understanding the potential modes of failure is crucial when designing a tool. The most predominate modes of die failure result from die overloading, wear, and overheating [3]. Die overloading is typically the less prominent mode of failure as loading conditions and limits are clearly identified during the design phase. Design factors that are considered to prevent failure from overloading are the use of a suitable die steel, block size, and working pressure; impression faces with smooth transitional surfaces and large radii; and proper seating of the dies in the forging press.

Die wear is unavoidable. It occurs due to the flow and displacement of hot metal in the impression; severity of wear increases with complexity of the impression geometry and increased forging temperature. Lubrication is applied prior to forging to lessen the frictional force between the work piece and the tool, minimizing die wear. During the current research project, two lubricants were considered: graphite or boron nitride lubricants. The graphite lubricant was selected and applied to the work-piece prior to forging as it was considered more effective and economically cheaper [10]. Separating the forging

operation into multiple stages and forging using blocker dies prior to completing the operation in a finisher die is another method that can be employed to drastically improve the life cycle of the die.

Heating a die causes the resistance to wear to decrease, leading to premature die wear. Die cavity regions closer to the heating elements are prone to overheating. An internal cooling system should be integrated to prevent overheating of these regions at high temperatures leading to heat checking [32]. Heat checking occurs in the corners or on projections in the die impression due to the variation in cooling rates between the centre and surface of the die. Once a crack appears, it grows with repeated forging cycles.

For the purposes of this research, tool wear was not considered during the design process since it was established very early on that only one hundred parts needed to be forged.

2.6 Forging Simulations

Methods employed to verify die fill include full scale die forging of prototype parts; metal flow patterns and occurrence of defects are identified and die designs are evolved through multiple iterations. This is costly in terms of time, material, facilities, and labour. The alternate, more prevalent method of modelling metal flow is through process simulations using finite-element method (FEM) based software. To simulate the anisotropic material behaviour of magnesium alloys under forging conditions, material flow curves as a function of strain rate, temperature and orientation are used to develop material models. Gou [7] and Paracha [10] performed magnesium alloy forming simulations using DEFORM 3D in the current research project. Modeling magnesium alloy deformation requires the inclusion of the anisotropic nature of the material. A Hill's Quadratic (6 coefficient) yield function was used to model material behaviour during forging. Coefficients used in the yield formula were acquired from uniaxial compression and shear hat testing for a range of temperatures and strain rates [33], with help from CanmetMATERIALS. Parameters such as stock orientation, friction coefficients, forging temperature and ram speed were determined by conducting a series of smaller forging trials. "Pancake" tests involving the compression of a cylindrical billet axially were carried out to compare the simulation and test loads. Ring-compression tests were carried to characterize the friction behaviour. "Flatbread" tests were conducted to observe the material deformation as a function of initial billet orientation in the as-extruded and transvers directions.

Finally, after developing complete anisotropic material models for distinct forging temperatures and

strain rates, numerical simulations of an I-beam forging designed to capture critical geometrical features present in the preliminary control arm design were carried out. Simulations were validated from I-beam forging trial results [10] [7].

2.7 Preform Design

A forging stock of a predetermined size and shape prior to the forging operation is known as a preform. The preform design is critical to achieving an adequate metal distribution and material properties in the final component. In practice, determining a proper preform design is difficult. Designing a preform allows control of volume distribution of the part as well as control over material distribution, with the objectives of achieving adequate die filling, minimizing material wastage and die wear by reducing metal movement, and achieving desired grain flow [11] to obtain suitable material properties.

Common practice in preform design is to first consider the final shape of the forging, and divide this geometry into axisymmetric or plane-strain flow regions. In a single or multi-step forging process, the volume of the forging based on the cross sectional area can be determined to derive a preform shape in the following manner as suggested by Altan for aluminum forgings [11]:

1. Consider the final forged component configuration, complete with flash.
2. Construct a baseline for determining the area parallel to the centreline of the part.
3. Determine the minimum and maximum cross-sectional areas perpendicular to the centreline of the part.
4. Plot the area values at proportional distances from the baseline.
5. Connect these points with a smooth curve.
6. At each cross section, add the approximate area of the flash above the curve.
7. Convert the minimum and maximum cross – sectional areas into round or rectangular shapes with the same area.

Figure 18: Preform: 63.5mm dia. x 716mm extruded AZ80 bar stock with a 108º bend angle

Preform design guidelines differ from material to material. In order to develop objective guidelines, understanding the material deformation mechanisms is essential. Preform designs were created and modified by the author in collaboration with Paracha [10]. The preform designs were used to conduct forging simulations using DEFROM 3D to predict the effect of forging temperature, strain rates, and billet orientation on the flow stresses and forgeability of the work-piece. The final preform shape which was used during the control arm forging operations is shown in Figure 18.

Chapter 3
Forging Tool Assembly Design

3.1 Design Overview

The hot forging tool development process was initiated by conducting a requirements analysis, and defining specifications by identifying functional requirements and design constraints. As shown in Figure 19, the subsequent steps are categorized into three major tool development stages. At the end of each stage, design debriefs were made to University of Waterloo APC Task groups, Multimatic Technical Centre, and CanmetMATERIALS. Refinements were made to the final conceptual design by Hendrik [34] from MTC. The final design was then approved by all parties for manufacturing.

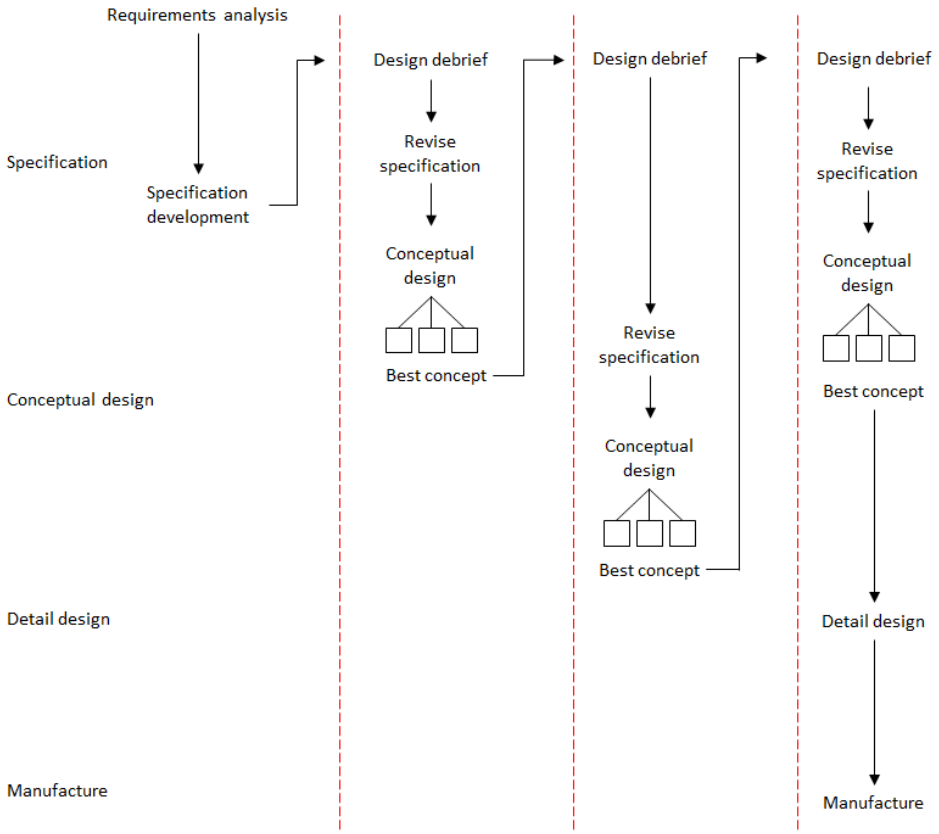

Figure 19: Tool development flow chart

3.1.1 Design Specifications

Functional requirements of the forging tool assembly were established during the preliminary design stage:

- The forming tool must consist of a component impression cavity
- The tool must be able to withstand a maximum load of 1600 tonnes (the max operating capacity of the 1500-tonne forging press at CanmetMATERIALS)
- Heating elements embedded in the tool must be capable of heating the tool to temperatures upwards to 350°C
- The tool must be capable of operating at elevated temperatures with limited heat loss during the forging process
- Thermocouples need to be installed in the tool for controlling and monitoring the tool temperature
- Tool design must be robust enough for installation in both the 1200 and 1500-tonne presses (Figure 20)
- Tool design must contain features for aligning upper and lower assemblies
- Tool must contain a component removal mechanism
- Tool must contain work-piece locating features

The spatial occupancy of the upper and lower tool assemblies were constrained by the dimensions of the forging press bolster or press bed, and by the open/shut heights of the punch and blank holders. Table 4 illustrates the critical dimensions for each press. The heating elements are powered by an existing 600V – 45 amp system with 6 control zones with a theoretical total power output of 27000 Watts. Power draw of heating elements is limited by the heating system. Each channel in the heating system provides feedback control; the system is required to have a minimum of two thermocouples to measure (and control) the temperature evolution [17].

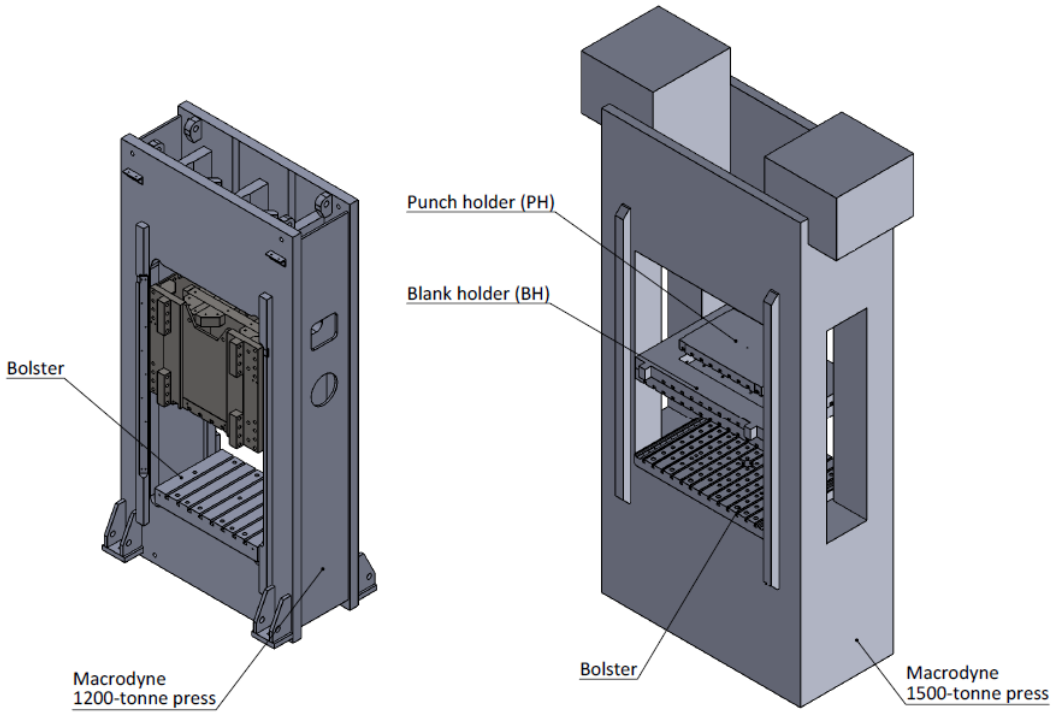

Figure 20: Macrodyne 1200-tonne & 1500-tonne presses at CanmetMATERIALS [17]

Table 4: CanmetMATERIALS-Forging press dimensions. (BH - Blank Holder, PH – Punch Holder) [17]

Forging press dimension	Macrodyne 1200 Ton Single-Action	Macrodyne 900/1500 Ton Triple Action
Open / shut heights (mm)	PH: Open: 1143 PH: Shut: 203.2	PH: Open: 1524 PH: Shut: 609.6 BH: Open: 1219.2 BH: Shut: 0
Dimensions (mm)	Bolster: 1397x914.4	PH: 1371.6x914.4 BH: 2133.6x1524 Bolster: 2133.6x1524

3.2 First Conceptual Design

An exploded view of the first conceptual design of the lower forging tool is shown in Figure 21, depicting the main components of the tool. A complimentary design was envisioned for the upper assembly of the forging tool. The focus during this stage was to develop a tool concept which would fulfill the following functional requirements: imparting the control arm shape, supplying heat to the forming surface, and providing a means of component removal from the tool (this functional requirement was omitted in the subsequent design iterations). The design was based in part on experience by Guo [7] designing a forming tool for the I-beam specimen.

CAD models were developed using SolidWorks 2013. Forming tool CAD were developed using both solid and surface modelling techniques. Boundary, ruled and loft surface tools were used in combination with multiple curve sketches defining the enclosure shapes to create the forming surfaces of the tool from the as-forged component geometry CAD. The multiple surfaces were stitched together using the knit surface tool and thickened to form a solid component. All other tool components were developed using purely solid modeling techniques. The component-level models were then assembled into the assembly-level model.

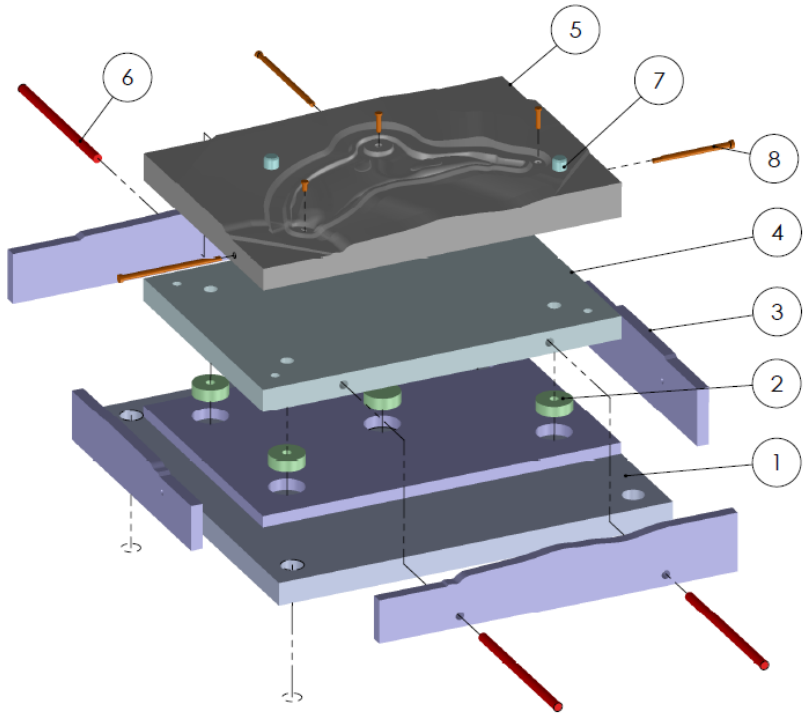

Figure 21: Exploded view of the lower forging tool showing key components (1st design iteration)

Key components comprising the lower forging tool assembly are called out in Figure 21. The forming tool **(5)** is supported by the heater plate **(4),** and accommodates ejector heads and rods **(8)** and alignment pins **(7)**. The thermal characteristics of the forming tool need to be controlled as they affect a number of aspects of the forging process. Additionally, the forming tool surface temperature must remain fairly uniform in order to produce a work-piece with a uniform temperature at the time of extraction in order to prevent distortion during cooling outside the tool. Hence, it was determined early on that incorporating a separable heater plate **(4)** would be beneficial. The heating elements used in the design are electrical resistance heating cartridges **(6)**. They are intended to be embedded in holes bored in to the body of the heater plate **(4)**. The heating elements can be separately controlled by an external system. The forming tool and heater plate are thermally insulated using insulation laminates **(3)** on the outside surfaces and the bottom surface of the heater plate (i.e., the surface opposite the forming surface) which rests on an unheated platen **(1**). The heater plate and forming tool are supported by steel pucks that are fastened to the bolster plate, which in turn, is fastened to the press bed. The bottom insulation is placed around load carrying columns or pucks **(2)** and between the heater plate **(4)** and bolster plate **(1)**, to limit heat conduction from heater plate to the platen. The first conceptual design was purposeful in establishing the overall size and the necessary key components of the forging tool.

3.2.1 Lower Forming Tool Design

The forming tool was created from the as-forged final control arm (13097-0000-2 R009) surface geometry. Geometric specifications of the impression cavity were verified indirectly by verifying the imprint surface of the control arm. Figures 22 and 23 illustrate sections of the control arm geometry near the deepest cavity and thinnest web regions, respectively. The validated geometry was then split in half along the periphery of the parting line as shown in Figure 24. The separated surface geometries were used to imprint the complimentary forming tool impression cavities. Table 5 shows the specifications to which the impression tool draft angles, radii, web and rib thicknesses were modeled. I-beam forming tools developed to these geometric specifications were used to produce successful forgings [7]. Thermal expansion effects at elevated temperatures were also taken into consideration; magnesium and steel have a 2:1 expansion ratio. Impression cavity volume was increased in proportion to the difference in the coefficient of thermal expansion of magnesium and steel in response to a temperature difference between

250℃ (optimal forging temperature) and room temperature. Therefore, the volume of the impression cavity was increased by 1% the total volume of the control arm

Table 5: Geometric Specifications (reproduced from [6])

Requirement	Case	Value
Outside Draft Angle (do)	>=	5 deg
Fillet Radius (ri)	>=	10 mm
Corner Radius (re)	>=	2.3 mm
Web Thickness (wb)	>=	5.0 mm
Rib Thickness (rb)	>=	6.35 mm

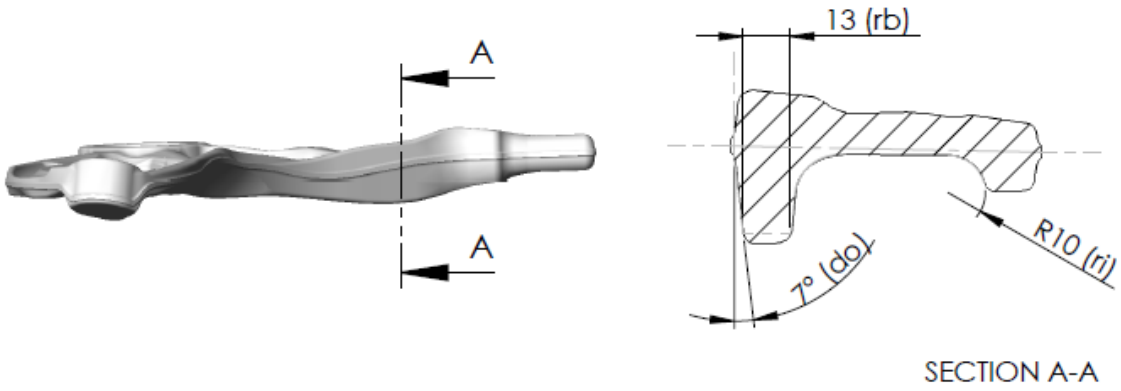

Figure 22: Section view of the deepest cavity region of the control arm geometry. (rb) rib thickness. (do) draft angle. (ri) fillet radii.

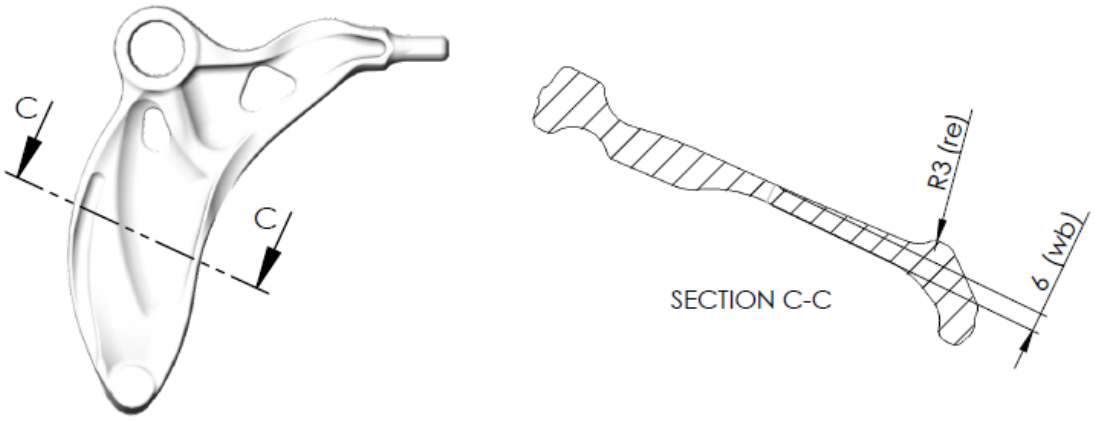

Figure 23: Section view of the thinnest web region of the control arm geometry. (re) corner radii. (wb) web thickness.

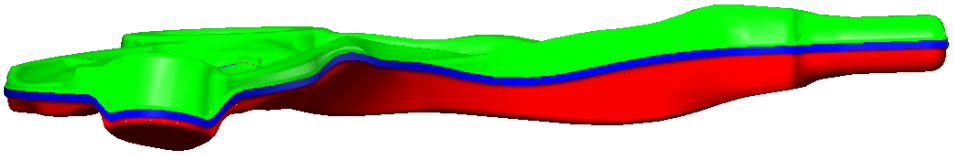

Figure 24: Impression tool - cutting surfaces. (Blue) 3.3mm thick parting line. (Green) upper impression surface. (Red) lower impression surface.

Flash dimensions of the first impression tool design were determined based on flash land and height equations provided in Chapter 2. Based on material forming simulations conducted by Paracha [10], flash land width was reduced from the initially estimated 10 mm to 6.5 mm, resulting in a reduction in peak forging load. The flash land height (the gap created atop the flash land when the upper and lower die mating faces are brought into near contact) was maintained at 3.3 mm. The gutter cavity depth and the gutter floor surface area were sized in order to contain a flash volume equivalent to 30% of the work piece volume. A system of holes was included in the design to contain the ejector pins and heads. The gutter wall ramp connecting the gutter floor and flash land was inclined at 135° angle to the gutter floor, as shown in Figure 25.

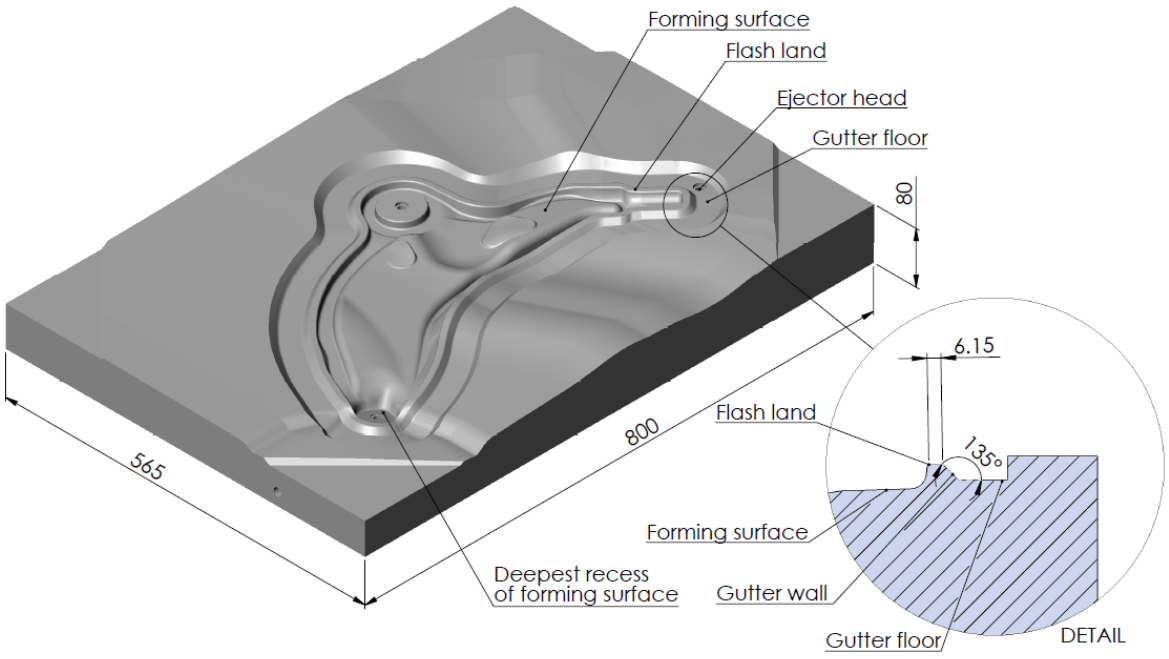

Figure 25: Lower forming tool (1st design iteration)

3.2.2 Heater Plate

The heater plate contains holes for housing the heater cartridges, which draw power from the heating system. The power is converted to heat energy and distributed through conduction. Based on engineering judgment, in order to promote a uniform temperature gradient over the forming surface, heating elements were positioned along the centre plane of the heating plate with their centerline offsets at 240 mm and 220

mm, as shown in Figure 26. The heater outside diameter (OD) is separated from the bottom surface of the forming tool (i.e., the surface opposite the forming surface) by 15.88 mm of steel. Cartridge OD is separated from the forming surface by 53 mm to 86 mm of steel as shown in Figure 27. The cartridge housing shafts were initially 356 mm in length, with an inside diameter (ID) of 19.05 mm.

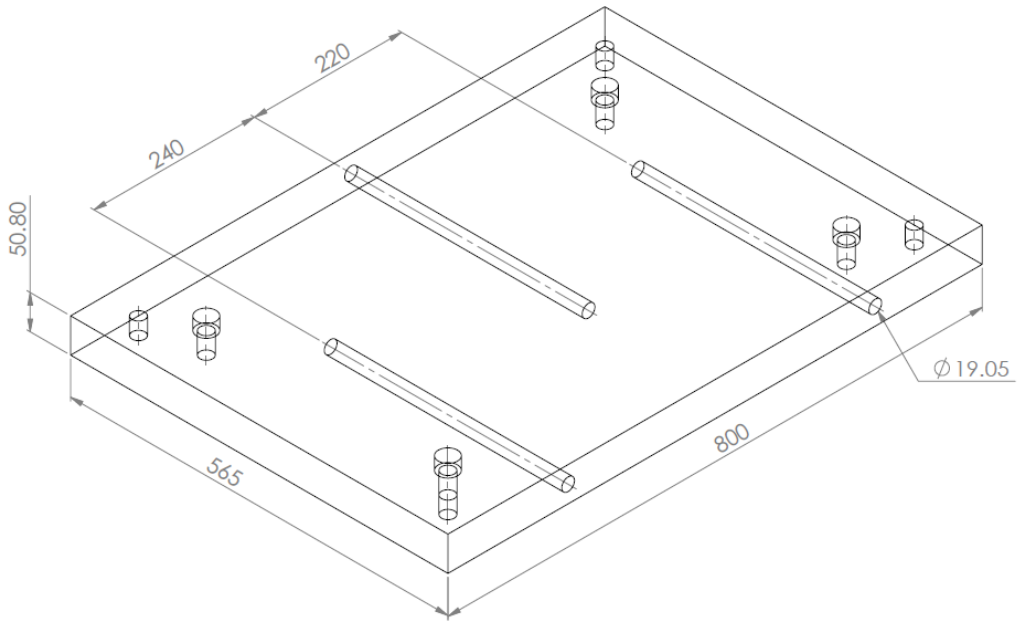

Figure 26: Isometric view of heater plate (1st design iteration)

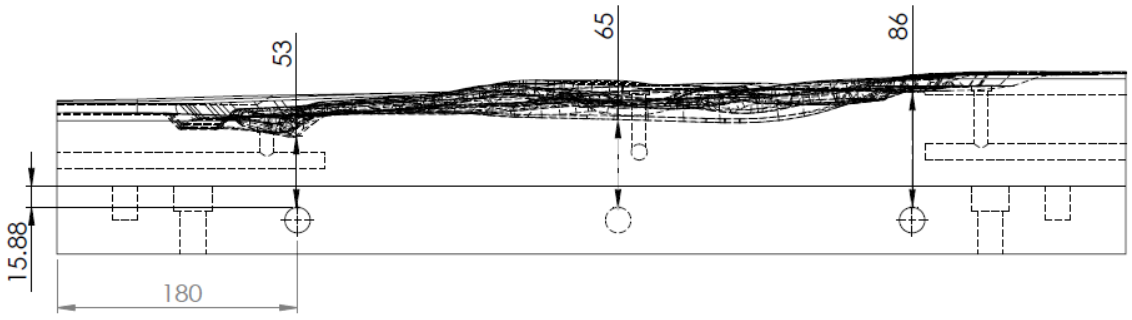

Figure 27: Side view of forming tool and heater plate

Each heater cartridge can be independently controlled; cartridge heating can be cycled by the controller to obtain uniform temperatures over the tool forming surface. Since upper and lower forming tools are similar in size and weight, analytical calculations were carried out to determine the amount of heat energy required to raise the temperature of just the lower forging tool from room temperature to 350°C. An assumption was made that tool heating would occur with both forming tools in a "closed" or "shut" position; the mating surfaces would be in close proximity, separated only by the height of the flash. Hence, the heat transferred to the surrounding environment from the top surface of the forming tool was neglected. Heat transfer to the surrounding environment from side and bottom surfaces were contained by a one inch thick insulation package. Heat transfer coefficients of the insulation laminates and surface orientation factors were determined from Omegalux supplier catalogues [35]. The heat energy lost to the environment at 350°C was combined with the heat energy required to raise the temperature of the lower forging tool from room temperature to 350°C. The heat energy was doubled to account for both the upper and lower forging tools, and divided by the number of cartridges. Heat energy output of a cartridge was divided by the number of hours anticipated to heat the tool, and based on this value; a heater cartridge model was selected from an Omegalux cartridge catalogue [35]. Model No. CIR-5142/240V was selected as a suitable cartridge type. Cartridge specifications are shown in Table 6. Analytical calculations are provided in Appendix A.

Table 6: Heater Cartridge Specifications

Specifications	Omegalux – Heater cartridge (Model No. CIR-5142/240V)
Wattage (W)	2500
Watt density (W/sq.in)	80
Leads	Type "F"; stranded, flexible manganese nickel wire insulated with fiberglass, max. temp 450°C (842°F)
Sheath	Material, Incoloy; black oxide finish for efficient heat transfer; max temp 816°C (1500°F)
Length	14 in. of heating sheath length with an additional inch of unheated sheath length. Leads insulated up to 842°F

According to the supplier, heater cartridges are typically slightly undersized relative to their nominal diameter. Close fitting tolerances were recommended in order to minimize air gap between the cartridge OD and the bore hole ID. Model No. CIR-5142/240V has an OD of 19.00 mm. It is also recommended by the manufacturer that heater cartridge operation be kept under the maximum rated capacity, and that multiple cartridges be used to provide an even heat pattern rather than using fewer higher wattage heaters [31]. The idea of using cartridges with different heat flux capacities was ignored in order to maintain consistency in the design.

3.2.3 Insulation

In order to contain the heat within the forming tool and prevent heat from dissipating in to the environment, the tool was packaged with insulation laminate. An inch thick, Cogetherm-M insulation type laminate was recommended by McKinley from CanmetMATERIALS [17]. The manufacturer recommends the use of this type of insulation for complicated geometries. It offers high resistance to pressure and is suitable for continuous operating conditions at service temperatures up to 500°C.

3.2.4 Support Pucks

Forming tools and heater plates are supported on five load-carrying support pucks. High temperature and strength Inconel alloys were initially considered for its relatively low conductivity. Pucks were sized in order to support the maximum tonnage applicable by the press. The pucks were arranged with four pucks positioned at the corners, and a central puck underneath the heater plate. The described puck arrangement is shown in Figure 21. Pucks were initially 25.4 mm in height and 50.8 mm in diameter. Puck size calculation formulae are provided in Appendix A.

3.2.5 Platen

The first design of the bolster plate or platen was created to define the overall dimensions, tool stack to platen, and platen to press bolster fastening locations. The overall dimensions were assessed to verify they are within the design boundaries. The length and width of the plate were 880 mm, and the thickness was 50.8 mm. Figure 28 illustrates the first platen design.

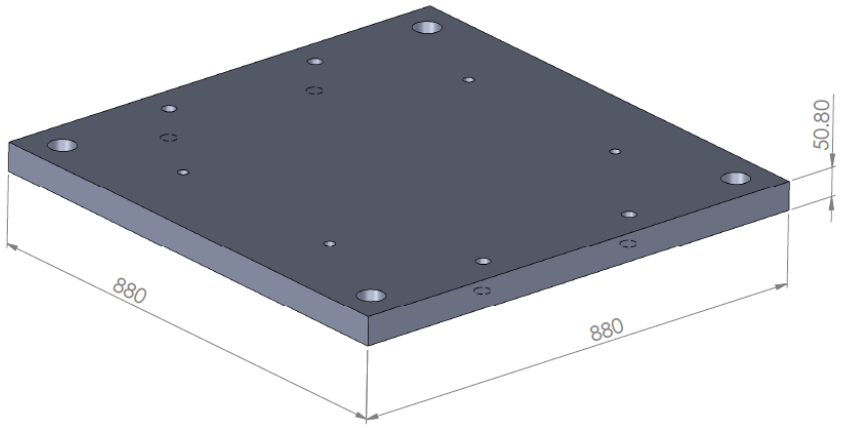

Figure 28: Basic platen design

3.3 Second Conceptual Design

During the second stage of development, a more detailed forging tool design was conceived. Following the preliminary design review, a decision was made to remove knockout pins; Strong [6] recommended they be used to facilitate rapid removal of the component from the die. This suggestion was made by MultimaticTECHNICAL based on industry practice. The flash containment gutter was also extended to the periphery of the forming tool to increase the flash containment volume as per suggestions by Dr. Lambert and Paracha [10]. The forming tool, heater plate, and insulation geometry were modified to accommodate pad retainers. Under advisement of Ron Champagne from MTC, the draft angle between the gutter wall ramp and gutter floor was also increased. Figure 29 and 30 show the upper and lower forging tool assemblies positioned in a vertically opposing configuration. The forming tool **(1)** and heater plate **(9)** were supported by the bottom insulation **(11)** and support pucks **(10)**. The puck arrangement was unaltered in this design iteration. Pad retainers **(12)** fastened the forming tool and heater plate to the steel

platen **(3)**, which was fastened to the bolster or press bed of the 1500-tonne press (not shown). The platen was raised above the bed of the press by a set of parallels **(4)**. The platen on the upper forging tool **(7)** mounted directly to the punch-holder of the press. The upper forming tool **(8)** and lower forming tool were aligned along the vertical closing axis of the press using an upper heel block **(6)** and a lower heel block **(5)**. Guide pin and bushing components **(2)** aligned the heel blocks. Figure 30 shows the maximum clearance height between the two halves of the tool for work-piece loading, along with the modified planar geometry of the tool.

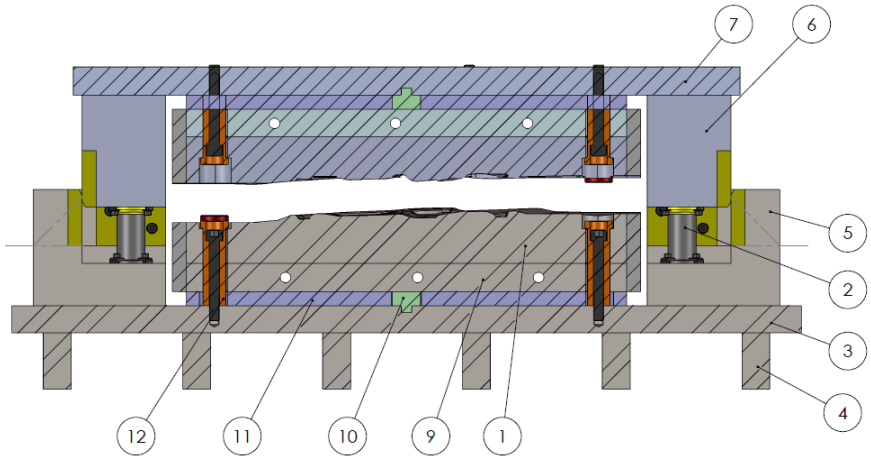

Figure 29: Forging tool side view cross section (2nd design iteration)

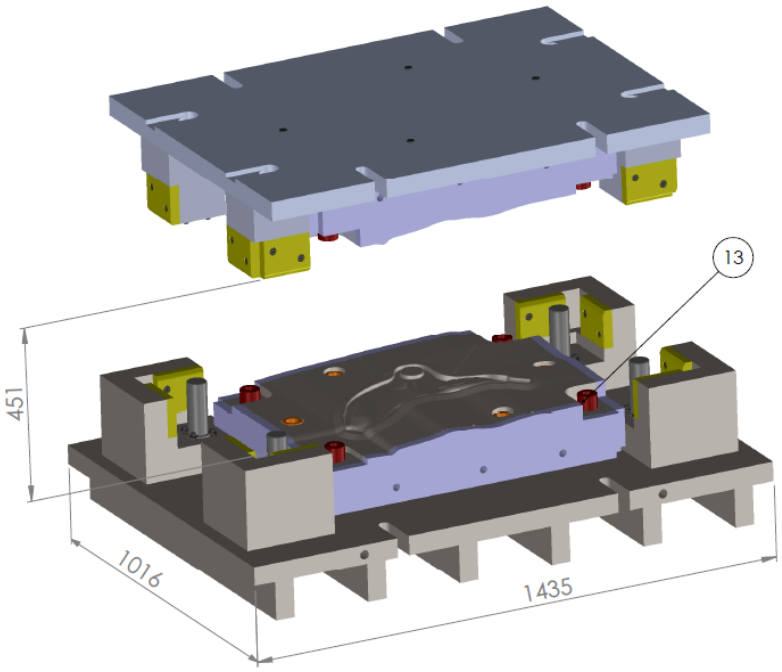

Figure 30: Forging tool second conceptual design

3.3.1 Upper and Lower Forming Tools

The second iteration of the forming tool consisted of an open (or unbounded) gutter floor. The unbounded gutter floor was modeled with smoother surfaces and larger fillets at intersecting flash land, ramp and gutter floor edges. Four oblong holes were positioned on the tool body as shown in Figure 31; clearance between the hole and the pad retainer allow for thermal expansion of the form tool. Horizontally aligned holes allow for expansion in the x-axis direction, and the remaining holes allow for expansion in the y-axis direction. Surfaces on the four corners of the tools were modfiied for mounting a die stopper. Die stoppers are used to ensure the upper and lower forming tools are correctly positioned at the end of the forging stroke. The gutter wall angle was increased to 158° from 135° in order to increase the rigidity in the wall region. The material was specified as untreated 4140 steel as per recommendations from Zwaan [34].

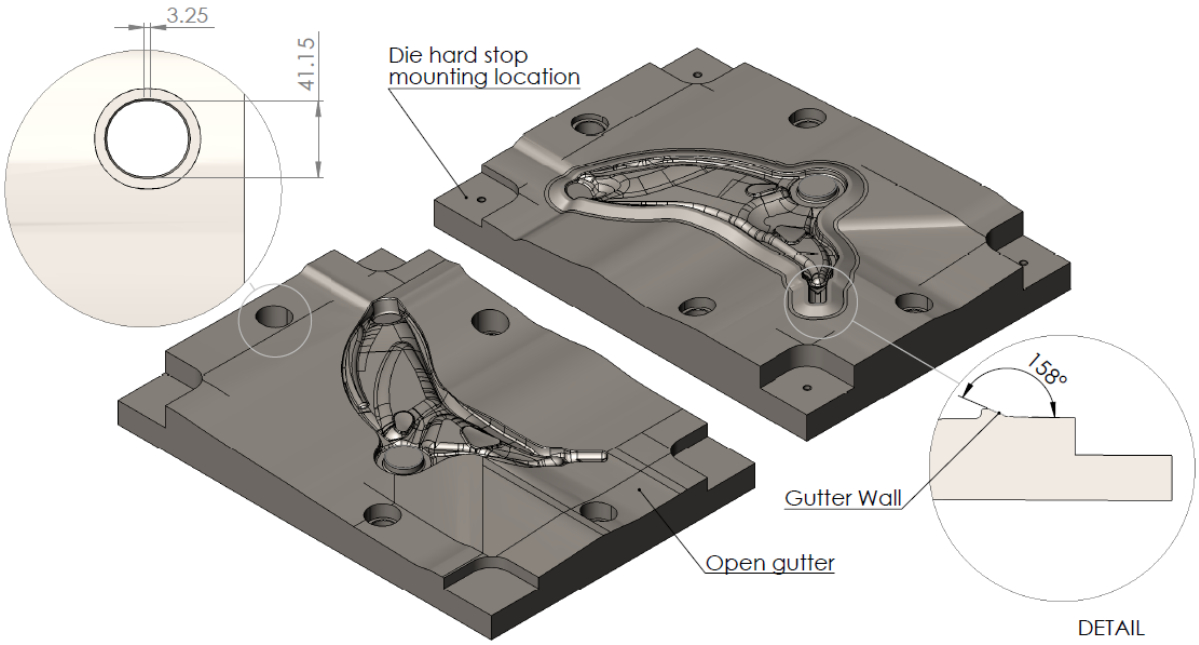

Figure 31: (Left) Upper Forming Tool. (Right) Lower Forming Tool.

3.3.2 Upper and Lower Heel Blocks

Self-lubricating wear plates, guide pins and bushings were sourced from a tool and die component manufacturing supplier, Anchor Lamina. Heel blocks as shown in Figure 32, were positioned on the four corners of the platens, to be welded onto the platen. A thin ventilation channel was machined into the upper platen, relieving trapped air pockets within the guide pin bore during die closure and action. Heel blocks increase the rigidity of the die assembly; die side thrust forces are resisted by the blocks, preventing misalignment of the upper and lower forming tools. Bronze self-lubricating wear plates were fastened onto the upper and lower heel block assemblies; graphite plugs cover 25-30% of the wear plate surface. The plates resist wear, abrasion, and deformation under high compressive loads [28]. They are recommended for use in applications dealing with high internal die forces.

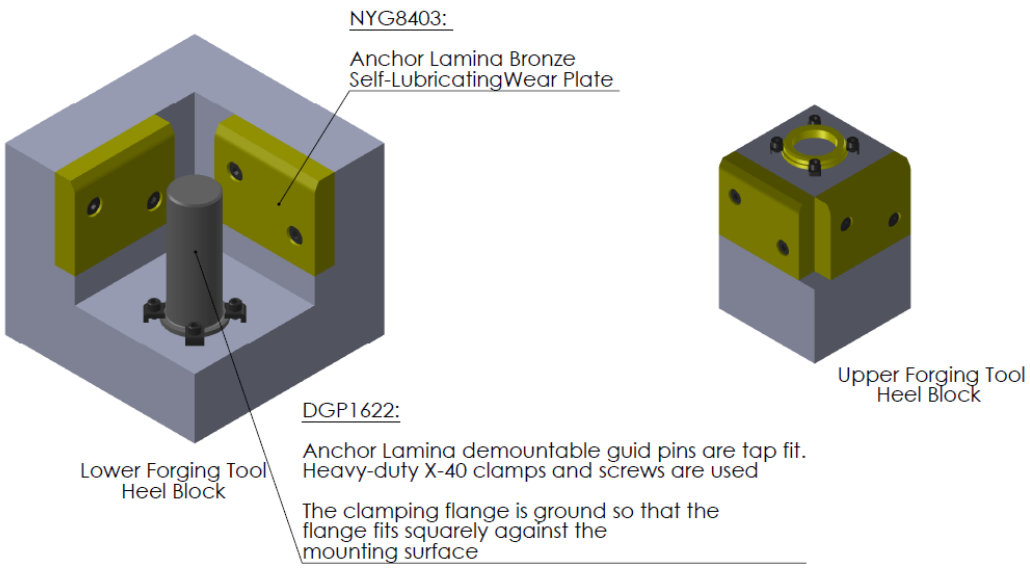

Figure 32: (Left) lower heel block. (Right) upper heel block

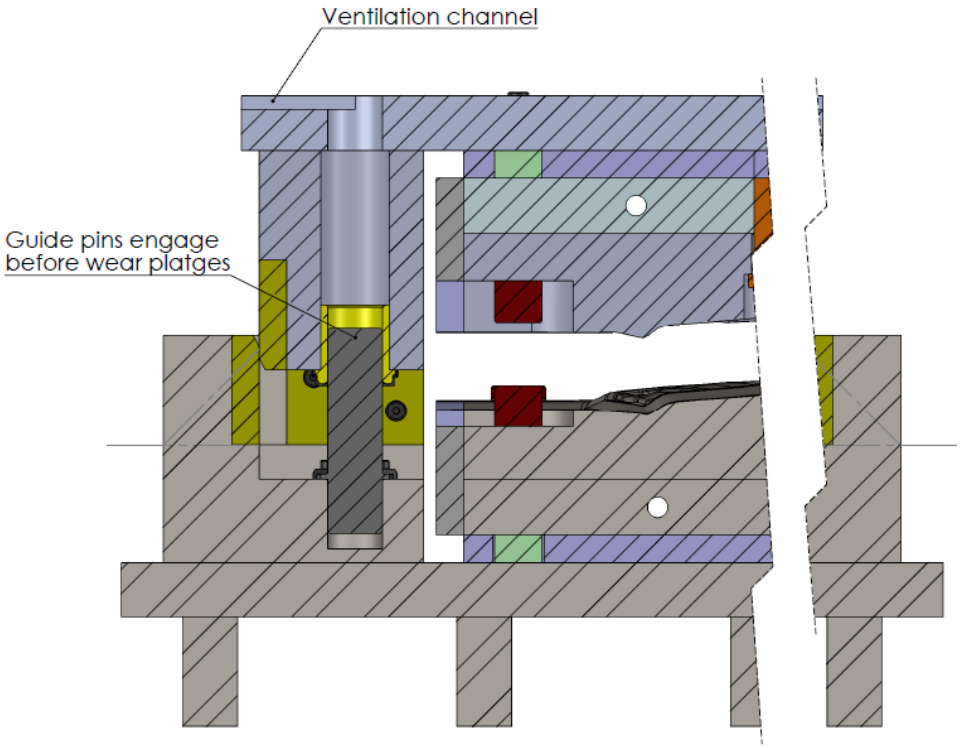

Figure 33: Cross section view of upper and lower tool engaged

Hardened steel, high-precision press-fit guide pins are clamped on to the four lower heel block assemblies via toe clamps and screws. Bronze plated bushings are tapped and clamped to the orifices of the four upper heel block assemblies. The guide pin and bushing engage first during die closure, ensuring upper and lower die alignment prior to work piece deformation. Figure 33 shows a cross-sectional view of the upper and lower heel blocks in the engaged position.

3.3.3 Second Heater Plate Design

The second iteration of the heater plate design contained heater cartridge holes that traveled through the entirety of the plate; straightness tolerances of ± 0.25 mm– specified for the cartridges – could be achieved as suggested by Mark Kuntz from University of Waterloo Engineering Machine Shop. Plate material was also specified as untreated 4140 steel. Oblong holes identical in dimension were positioned to align with holes in the forming tool. Overall dimensions of the heater plate were not altered.

3.3.4 Second Platen Design

The lateral length of the platen was increased to accommodate the heel blocks. Parallels were added to the model, welded to the bottom surface of the platen. Parallels were spaced and sized to facilitate forklift access. Both the front and back side surfaces of the platens are threaded for eye bolt installation; cables can be tied to the eye bolt collar in order to guide the die assembly during the installation process. U-shaped slots were cut into the platen along the length of the plate at locations which are axially aligned with the press bolster T-slots. Fasteners secure the platen to the bolster along the T-slot track. Similarly, the upper platen fastens to the press punch. Figures 34 and 35 illustrate the CAD models of the two components.

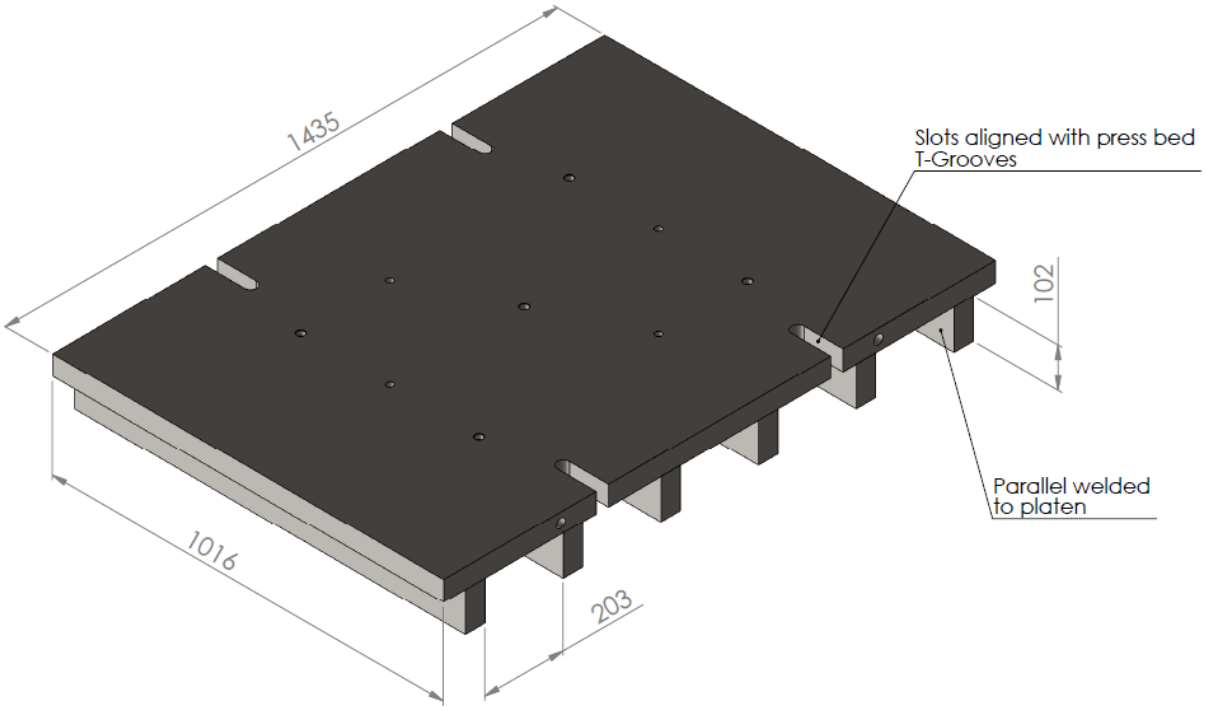

Figure 34: Lower Platen (2nd design iteration)

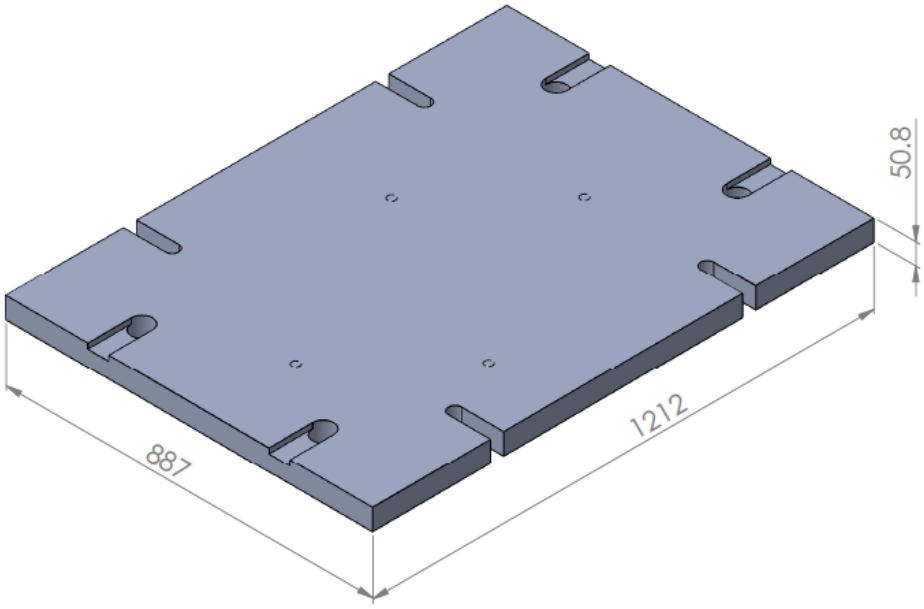

Figure 35: Upper Platen (2nd design iteration)

3.4 Third Conceptual Design

Modifications were made to the overall tool CAD model in the third design iteration to increase the fidelity of the model. Feedback from the second design review led to modification of the forming tool **(1)**, pad retainer locations **(2),** heel blocks **(3)**, and keys **(4)** as shown in Figure 36**.** Guide pins and bushings were removed from the heel block assembly under advisement of MTC; tool alignment through wear plate contact was considered sufficient. Puck size was modified, and two extra pucks were added to the assembly as shown in Figure 37 for extra support. Pad retainers were re-located to the four corners of the forming tool to promote a uniform thermal expansion as suggested by Zwaan [34]. Keys and keyway features were added to align and connect the components during assembly, while still allowing for differential thermal expansion. Hard stops were replaced with large bolt heads which could be readily adjusted to the desired height.

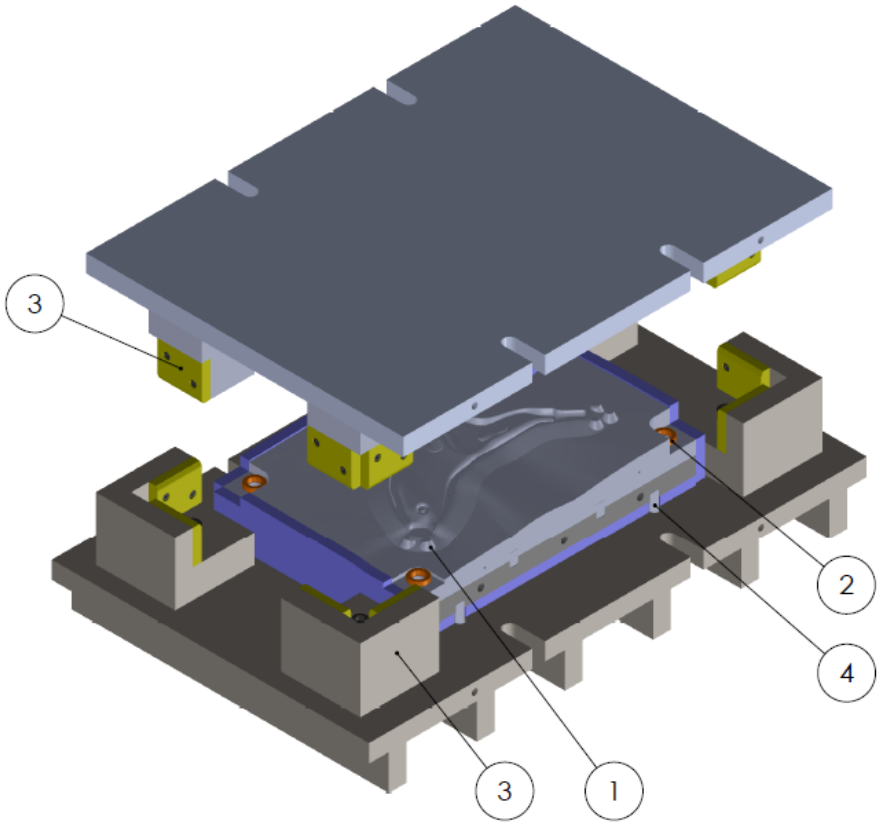

Figure 36: Forging Tool Assembly (3rd design iteration)

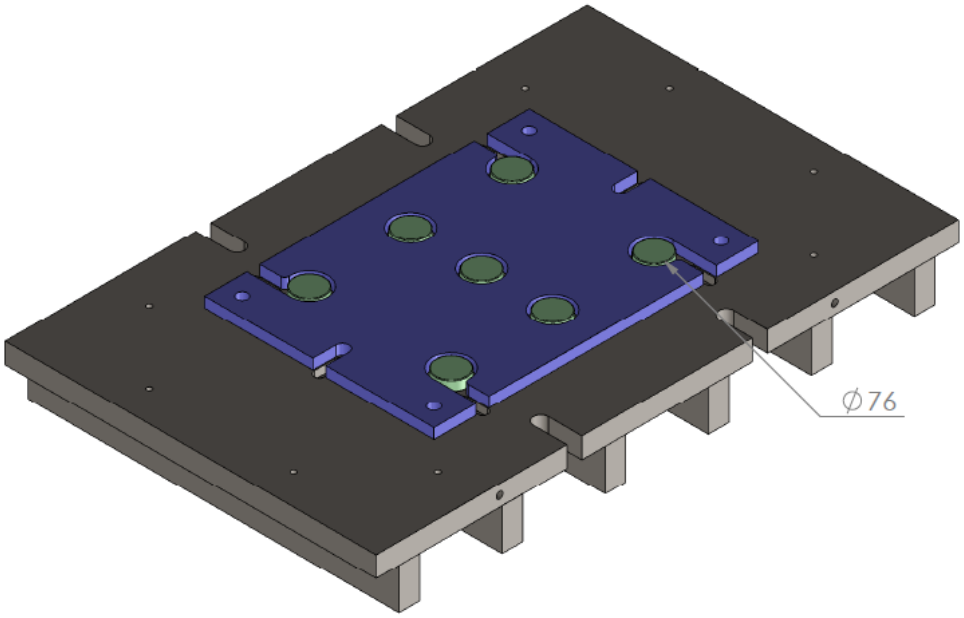

Figure 37: Puck arrangement modification

3.4.1 Upper and Lower Forming Tools

Modifications made to the upper and lower forming tool models are shown in Figure 49. Locating features – used to locate the as-forged component on a jig for post-forge machining operations – were added to the impression cavity of the lower die. Feature 50. Work-piece locating features are intended to locate the billet on the forming tool as shown in Figure 18. The machined surfaces on the conical prongs form a "V-groove" onto which the cylindrical billet is seated. Billet positioning is critical as it dictates cavity filling and tool wear (tool wear was neglected for this application). Thermocouple bore holes and Ffikeyways were also added to both the upper and lower tool. The open gutter surface geometry was also smoothed and fillets were added to any sharp edges at gutter-cavity intersecting surfaces.

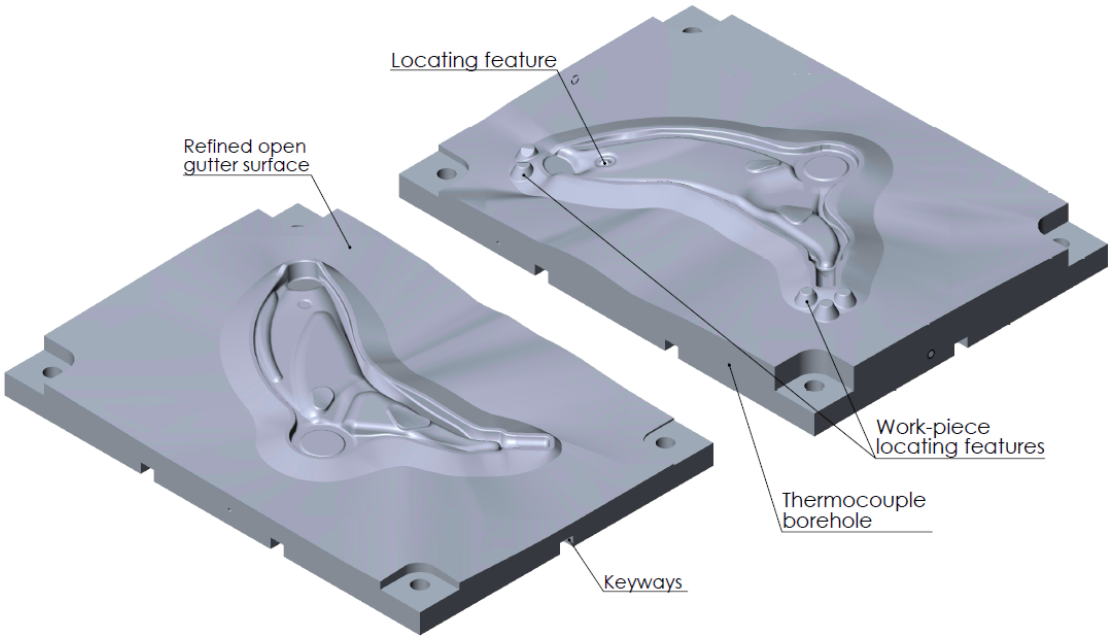

Figure 38: (Left) upper and (right) lower forming tool (3rd design iteration)

3.4.2 Second Support Puck Design

Puck diameter was increased to 76 mm and the configuration was modified to incorporate two additional pucks. The resultant configuration is shown in Figure 37. The height of the pucks was also reduced by 1.6 mm to a height of 23.8 mm, creating an air gap between the heater plate and puck contact surfaces. During the heating step – under no-load conditions – the tool is supported by the bottom insulation. By eliminating or reducing the contact pressure between the heater plate and pucks during the heating process, conduction heat transfer through the puck is reduced, promoting faster tool heating time.

Chapter 4
Detail Design and Verification

4.1 Detailed Design Geometry

The third conceptual design iteration for the die set was finalized by Hendrik Zwaan from MultimaticTECHNICAL. Overall dimensions of the forging tool remained unchanged. Modifications were made to the side insulation laminates to simplify the geometry. Fastening holes were added to the side insulation laminates and corresponding mating components. Oblong holes travelling through the height of the impression die and heater plate were modified; a 2mm clearance was created between the pad retainer OD and hole ID. The forming tool and heater plate are allowed to expand diagonally at each of the four corners as shown in Figure 39. The open gutter surface on the upper and lower forming tools was modified in order to reduce manufacturing costs. Heel blocks were welded onto the platen. The geometry of the lower platen and parallels were modified, and the parallels welded to the platen. The lower platen has material removed from the two side lengths in order to provide access to the fastening slots in the parallels below, as shown in Figure 40. Four height adjustable hard stops were added to the lower heel blocks. Nine support pucks were arranged in an identical pattern in both upper and lower forging tools, as shown in Figure 41. Chamfers and fillets were added to the entire model. All steel components were specified as untreated 4140 steel. Cogetherm-M laminates were used to insulate the tool. Three Omega, BT-090-K-8-60-2 thermocouples are inserted into bore holes in the forming tool for both the upper and lower tools. Three Omegalux CIR-5142/240V type heater cartridges are inserted into the upper and lower tools. Figure 42 shows the upper and lower tool being assembled at Multimatic Technical Centre.

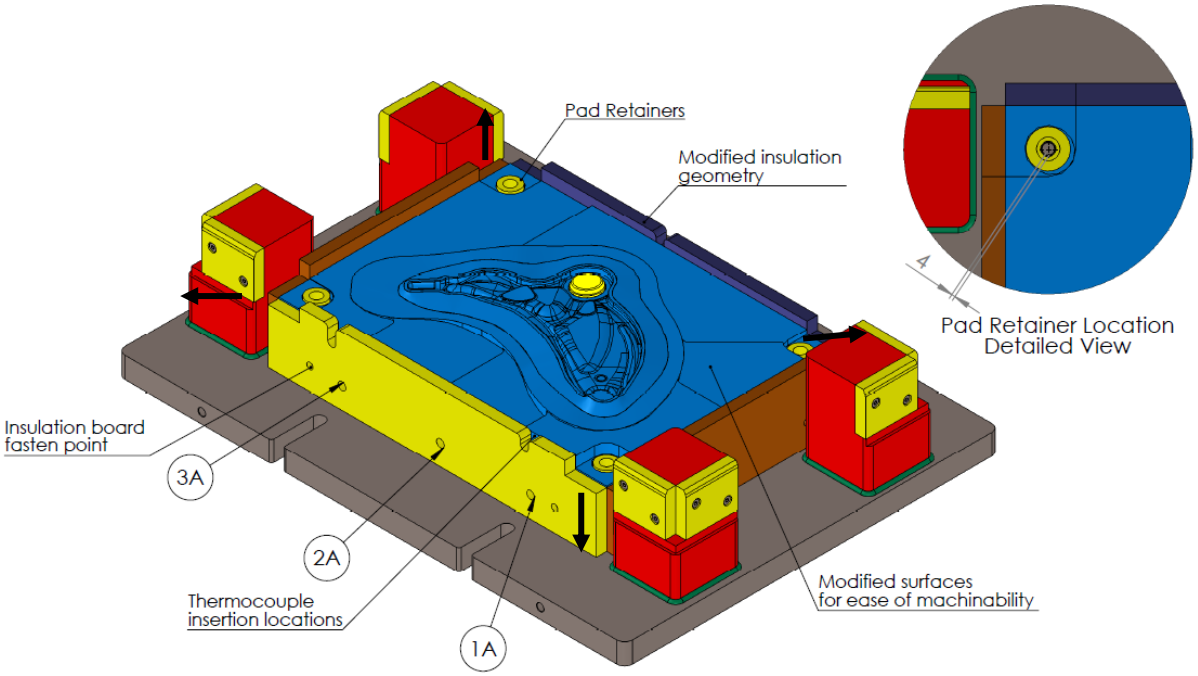

Figure 39: Upper forging tool (reproduced from [36])

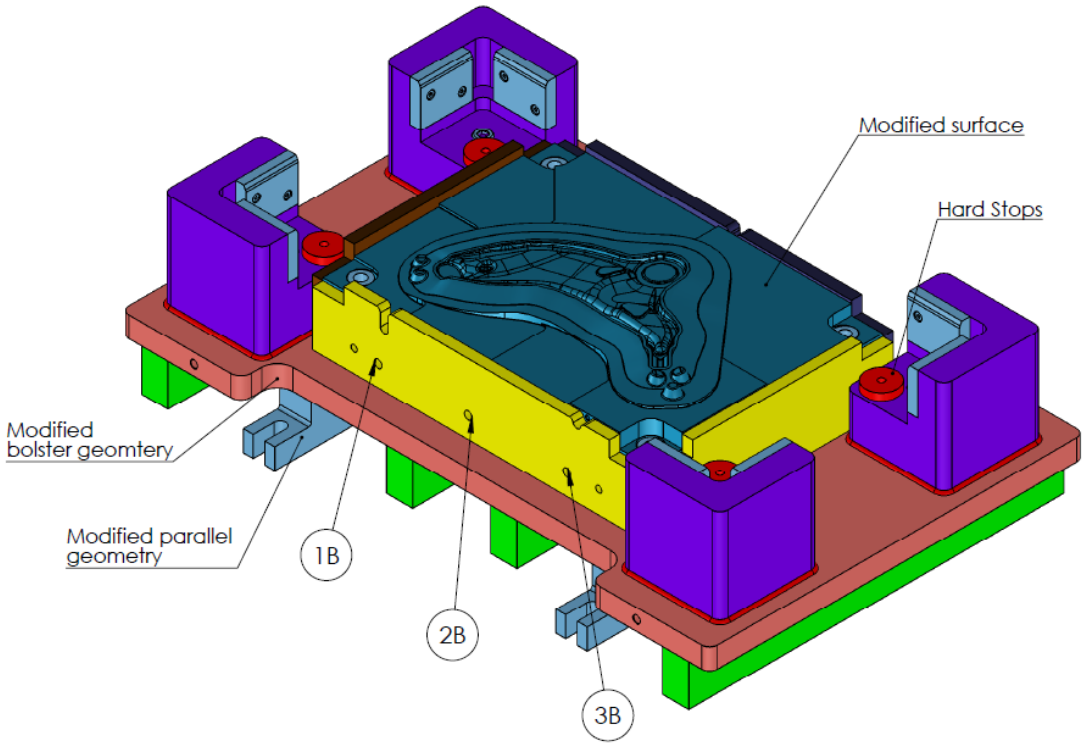

Figure 40: Lower forging tool (reproduced from [36])

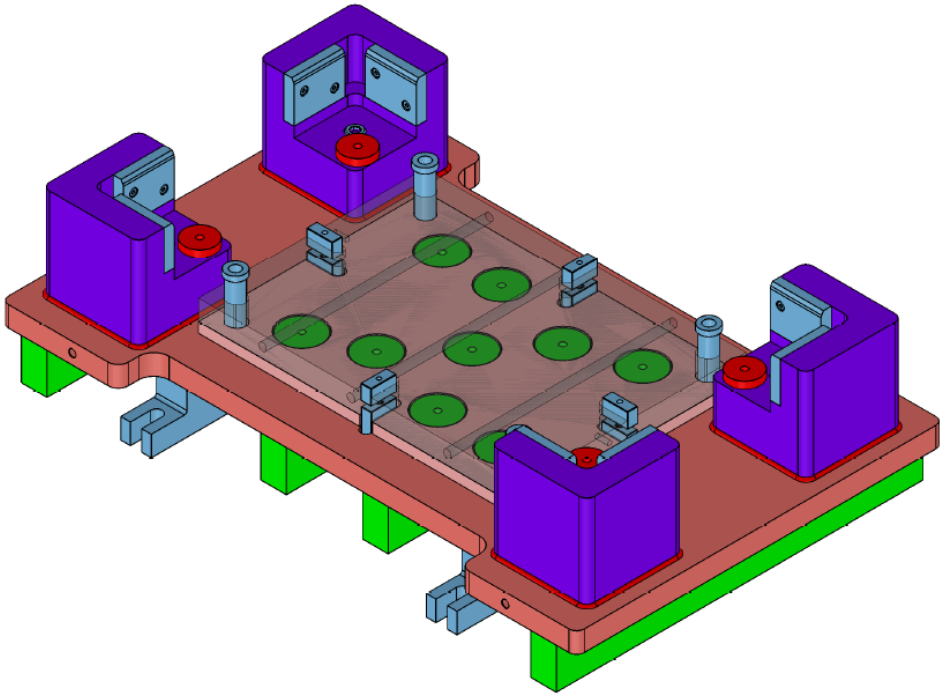

Figure 41: Puck configuration is shown (reproduced from [34])

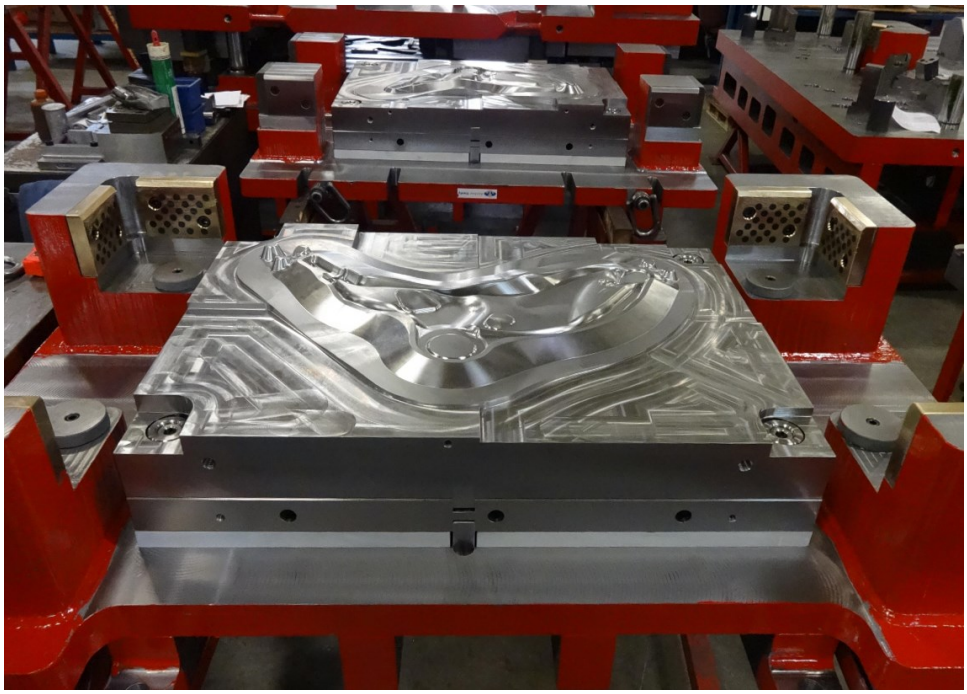

Figure 42: Upper and lower tools being assembled at Multimatic Technical Centre

4.2 Thermal Analysis

The detailed tool design was subjected to a heat transfer analysis. Heat transfer is governed by three effects: conduction through contacting surfaces, convection through the surrounding air, and radiative exchanges between exposed metal surfaces and the environment. Tool heating was simulated in a series of transient heat transfer steps [36]. The final die geometry was simplified and de-featured. Thermocouple holes, eye bolt and threaded holes, heel blocks, the pad retainer, and keys were omitted. The forming tool was partitioned into two volumes. The volume containing complex impression surfaces were meshed with uniform single order tetrahedron elements with a target mesh size of 5 mm. The remaining geometry of the tool was modeled with brick elements with a target mesh size of 10 mm. The bolster was modeled with the same brick elements, but with a mesh target size of 20 mm. The forging tool geometry was meshed using Hypermesh v13.0 and exported as an Abaqus '.inp' file containing nodes and volume elements [37]. Element types were assigned in Abaqus CAE. Elements were assigned Abaqus DC3D4 and DC3D10 heat transfer element types. Surfaces in contact were defined using tie constraints. The forming surfaces of the upper and lower tools are exposed to hot air between the impression cavities when the tool is in the closed configuration. Heat conductance through the air gap was considered by assigning a gap-conductance property in line with a surface-to-surface contact definition between the upper and lower forming tool surfaces [37]. Surface-to-surface contact between the heater plates and support pucks were also modeled by applying gap-conductance properties. Outer surfaces of the insulation package exposed to the environment had a constant heat loss defined using a surface-based film condition. Sink temperatures were defined as $25℃$, representing the assumed ambient conditions. A film condition coefficient value of $1 \times 10^{-5} \frac{W}{mm^{2}\cdot℃}$ was used. A temperature boundary condition of $25℃$ was applied to the upper and lower tool platen surfaces in contact with the press bed. Material properties and boundary conditions were simplified. Radiation interaction between the platens and the environment was defined through a surface radiation to ambient interaction with an emissivity factor of 0.76 for the steel. A uniform heat flux load of $0.124 \frac{w}{mm^{2}}$ was applied to the heater plate cartridge bore hole ID. Six heat flux loads were applied to heat the forging tool. A predefined uniform temperature field, $25℃$, was applied to the entire model during the initial step of the simulation.

The temperature field over the upper and lower forming surfaces are shown in Figures 43 and 44, respectively; a temperature range is specified for clarity. After a 3.4 hour heating cycle, the nodal temperatures of the impression cavity in the upper tool ranges between $375℃$ and $420℃$. Similarly, after

3.75 hours of heating, the nodal temperatures of the impression cavity in the lower tool ranges between 375℃ and 440℃. Simulation results show a non-uniform temperature field over both forming surfaces. This is undesirable as regions showing large temperature gradients are susceptible to heat checking. Since these regions are also in contact with the work-piece, a similar non uniform temperature distribution occurs in the work-piece, resulting in non-uniform shrinkage of the component during cooling.

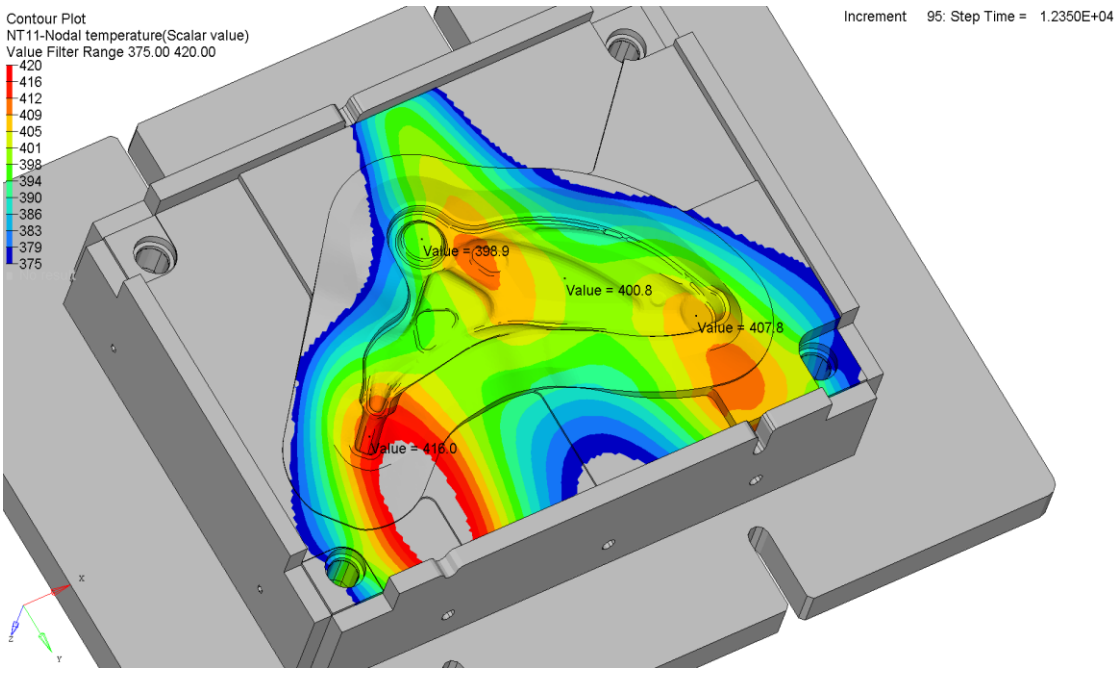

Figure 43: Temperature field over forming surface (upper tool). Heating time: 3.40 hours

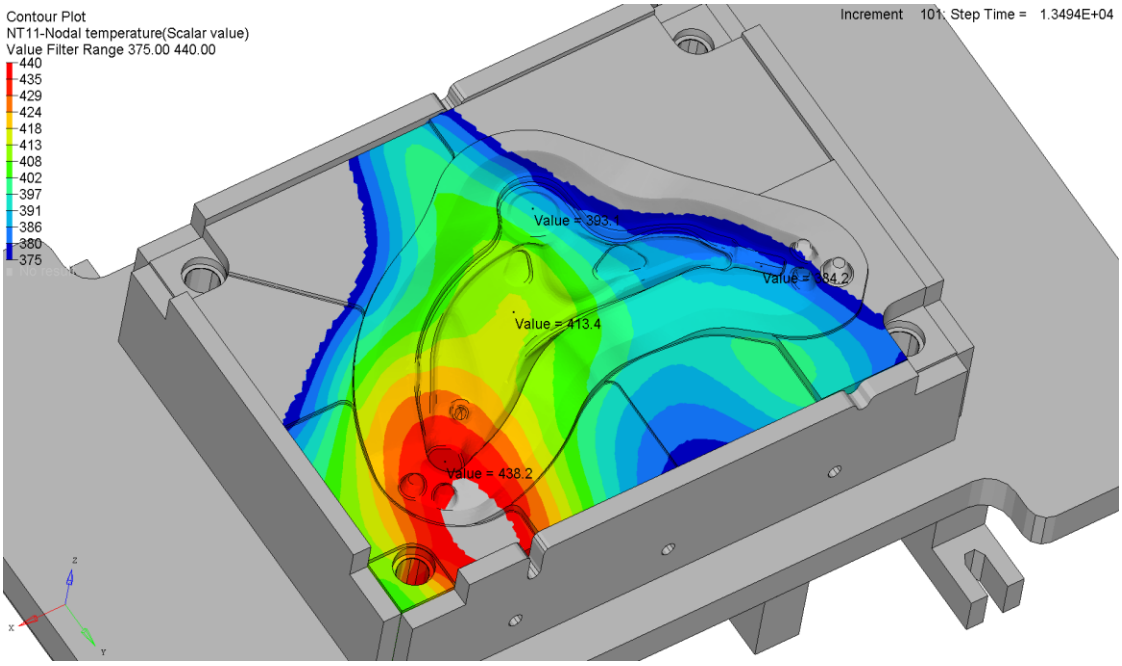

Figure 44: Temperature field over forming surface (lower tool). Heating time: 3.75 hours

Based on the temperature field distribution results, a control strategy is suggested to control the temperature of hot spots in order to obtain a more uniform temperature field over the forming surface. Cartridge activation times are suggested to minimize the temperature gradient over the forming tool surfaces. Figures 45 and 46 show the results of a heating simulation carried out to the heater cartridge duty cycle schedule specified in Table 7; cartridges are identified in Figures 39 and 40. The results show a more desirable temperature field after independently controlling cartridge heating times. Nodal temperatures over the upper tool ranges between 385℃ and 415℃, and in the lower tool, between 370℃ and 400℃. The upper tool is on average 10 degrees hotter than the lower tool. As shown in Figure 46, the highest temperature in the tool is observed on cartridge 3B, at the borehole opening.

Table 7: Heater cartridge duty cycle

	1	2	3
A	3.4 hrs	3.5 hrs.	3.4 hrs
B	3.4 hrs	3.5 hrs	3.75

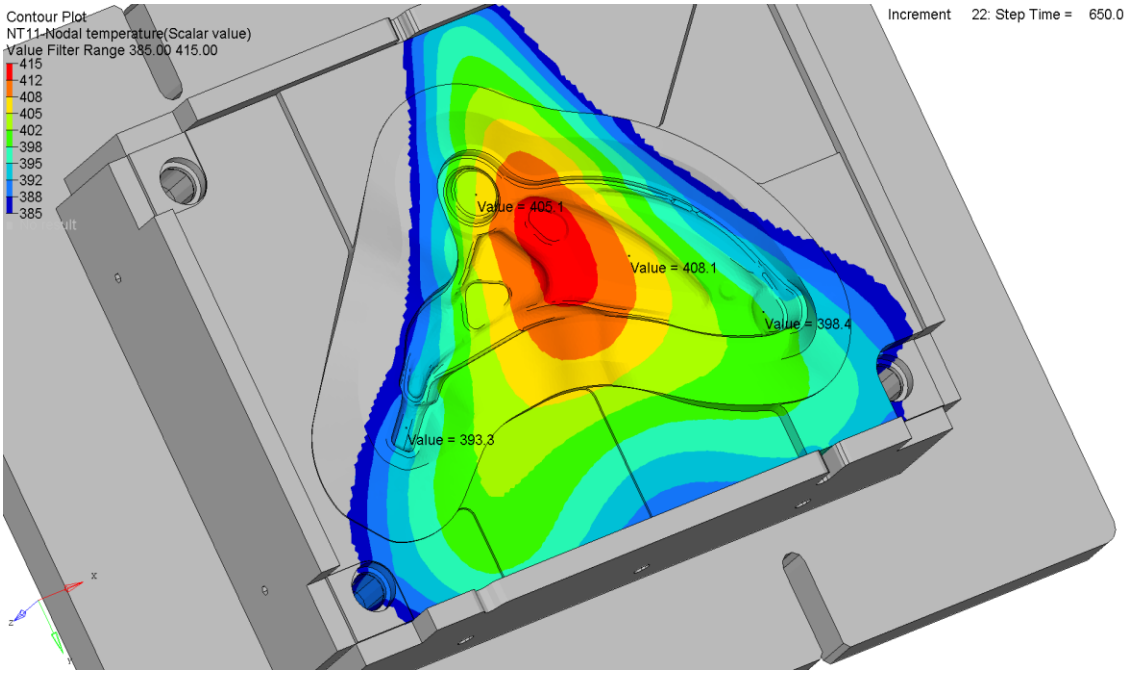

Figure 45: Temperature field over forming surface (upper tool)

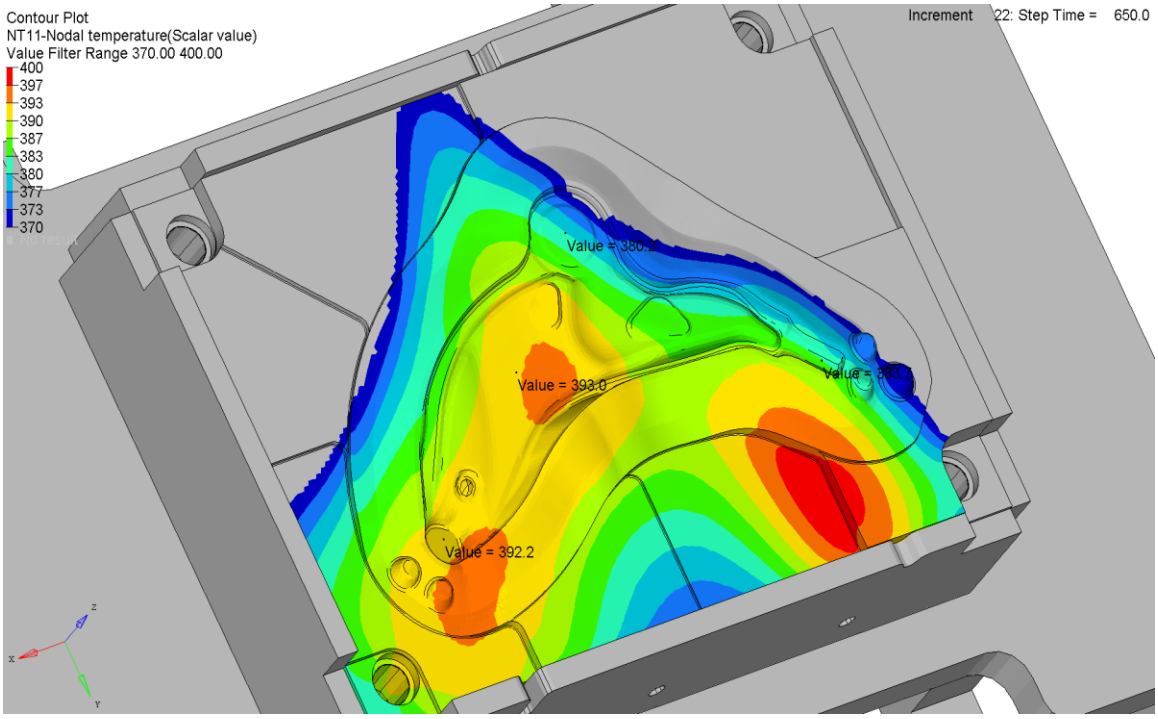

Figure 46: Temperature field over forming surface (lower tool)

4.3 Structural Analysis

A linear static analysis was performed on a low-fidelity model of the tool in order to evaluate the overall deflection and stresses under the maximum loading condition of 1600 tonnes. The forming tool partition containing the impression cavity was meshed using C3D4 tetrahedral elements and the remaining components were meshed using reduced integration, C3D8R brick elements; these elements account for geometrical material nonlinearities and minimize computational expense [38]. The bottom insulation was tied to the bolster, and the bolster to the parallels. Similarly, the pucks were tied to the bolster and heater plate, and heater plate to the forming tool. Tie constraints were created based on a surface-to-surface formulation to avoid stress noise at tied interfaces [40]. The press bed was considered rigid, and so boundary conditions were applied to the parallel or die shoe surfaces in contact with the press bed, constraining nodal displacement in U1, U2 and U3 directions. Steel components were assigned 4140 steel material properties. The insulation was assigned Cogetherm-M material properties (refer to Table 8). The predefined temperature field shown in Figures 45 and 46 was applied at the initial step of the simulation and the tool was subjected to load case in the subsequent step. Figure 47 shows the contact region between the preform and the forming tool captured from a material flow simulation performed by Paracha[10] for an AZ80 alloy at 400℃ under a peak forging load of 900 tonnes. The load case used in this low-fidelity model does not map the nodal pressures from this flow simulation on to the forming tool surface, since they were not available. Instead a uniform pressure of 170 MPa was applied over the contact region of the forming tool. The pressure was obtained by dividing the maximum press load of 1600 tonnes, or 15.7 MN by the contact area. This model does not accurately capture the loads acting on the tool, but was considered a reasonable approximation. In addition, since the pucks are connected to the model via tie constraints at the contacting surfaces, translation of the tied nodes are restricted, potentially leading to an over-prediction of stresses. At the time, this lower-fidelity model was considered sufficient in order to determine the peak stresses, and proceed within the project timeline.

Table 8: Material Properties

		Cogetherm-M [41]	4140 Steel [42]
*Density $\left[\frac{kg}{mm^3}\right]$		2.15E-06	7.70E-06
Young's Modulus $[MPa]$	20℃	-	210000
	100℃	-	205000
	200℃	-	195000
	300℃	-	185000
	400℃	172	175000
*Yield Strength $[MPa]$		250	650
Conductivity $\left[\frac{w}{mm-℃}\right]$	100℃	0.00015	0.043
	200℃	0.00017	0.042
	400℃	0.00020	0.037
Specific Heat $\left[\frac{J}{kg-℃}\right]$	200℃	-	473
	400℃	886	519

*Mechanical properties defined at 400℃

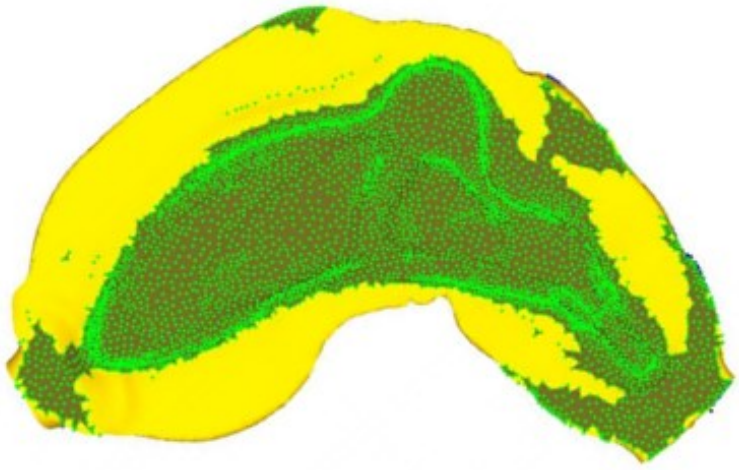

Figure 47: Deformed AZ80 preform at **400**℃ under 900 tonne peak load. Preform and forming tool contact region is shown in green (reproduced from [10])

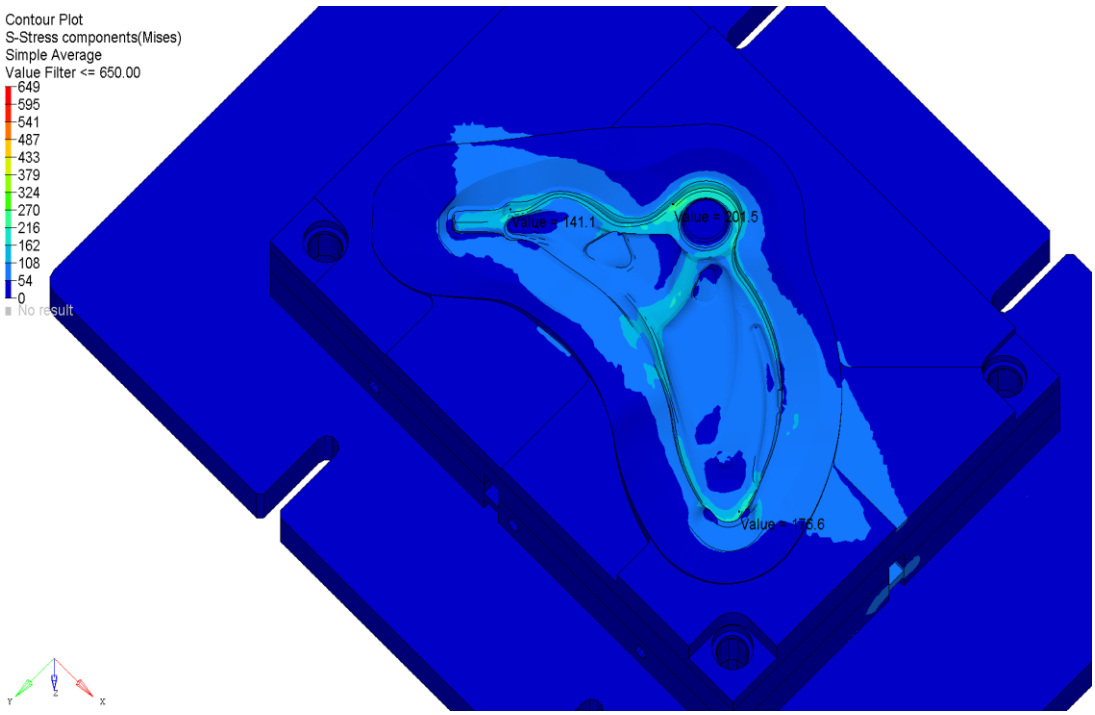

Figure 48: Von Mises stress contours on upper forming tool surface. Max value = 201 MPa.

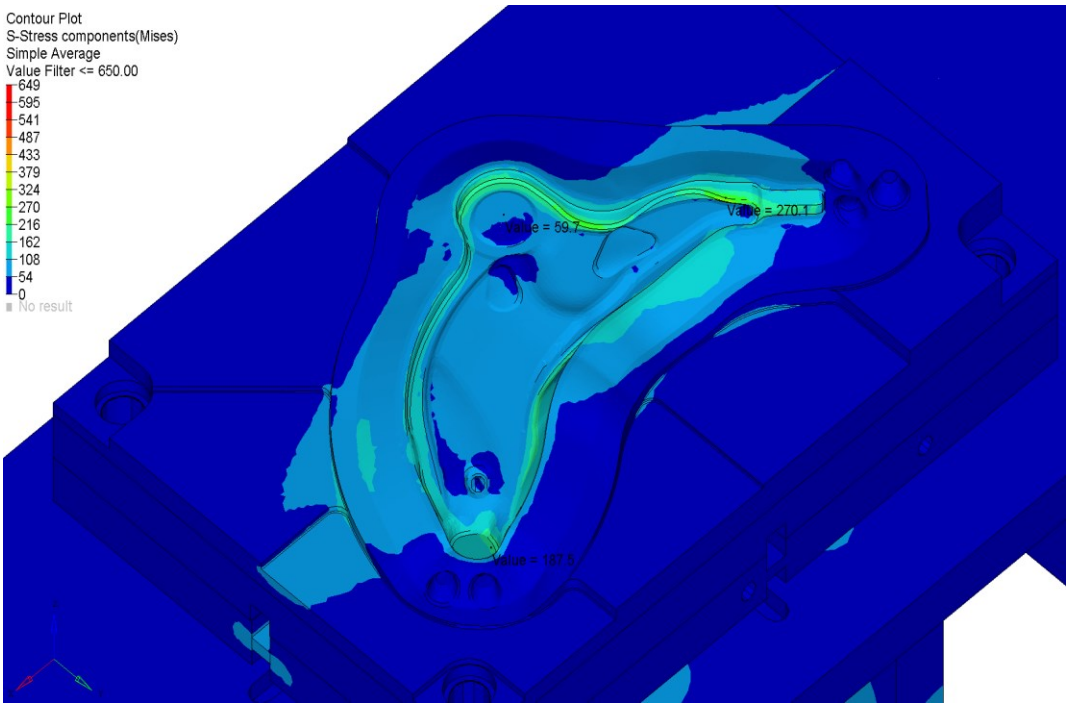

Figure 49: Von Mises stress contours on lower forming tool surface. Max value = 270 MPa.

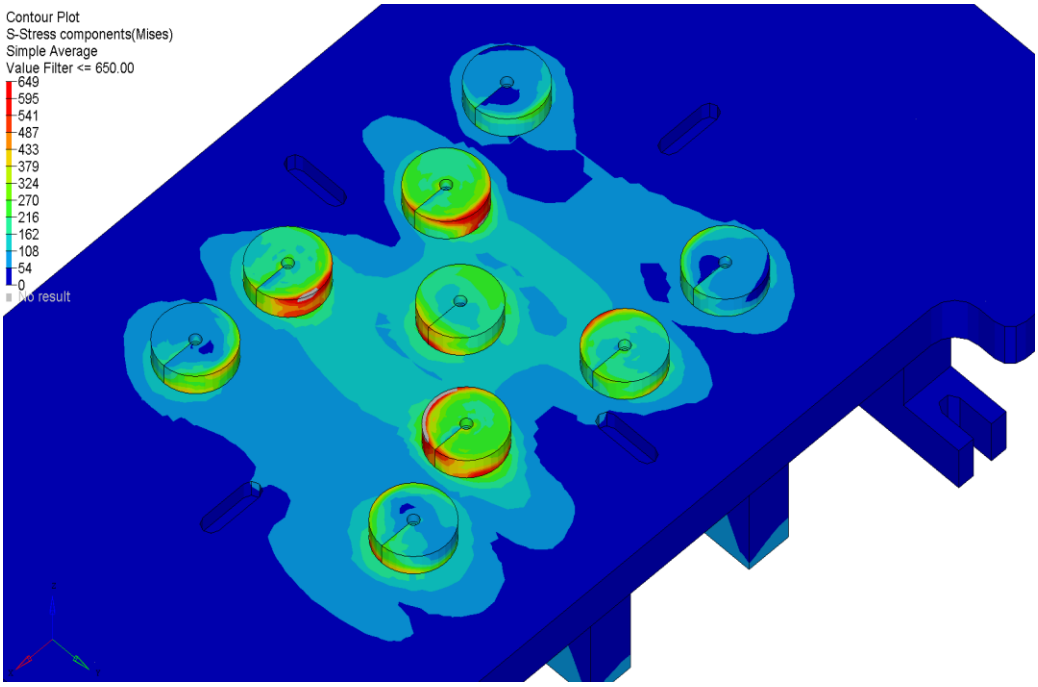

Figure 50: Von Mises stress contours on lower tool support pucks

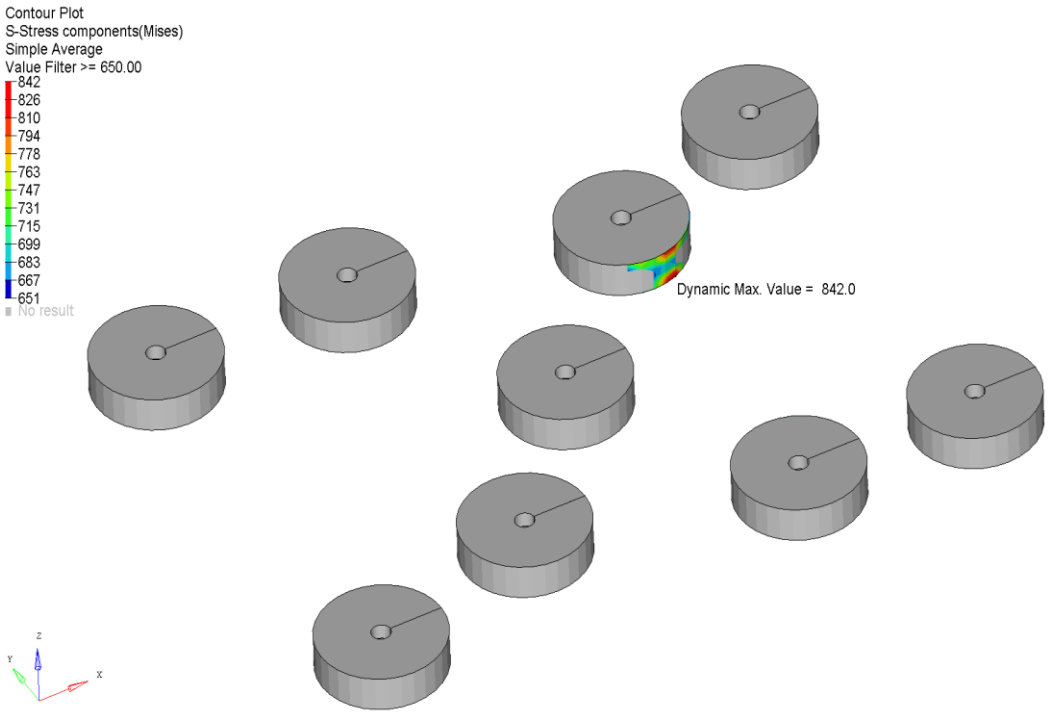

Figure 51: Support puck yield location (lower tool). Max value = 842 MPa.

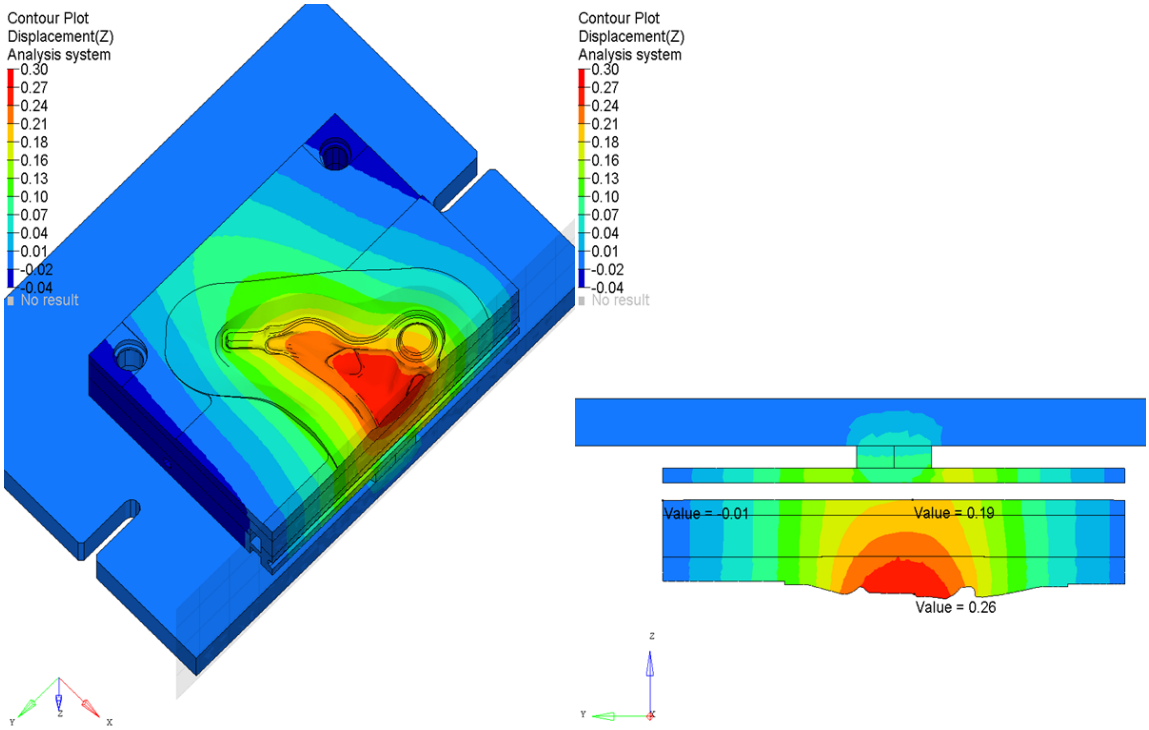

Figure 52: Upper tool nodal displacement (Z-direction). Max value = 0.26 mm

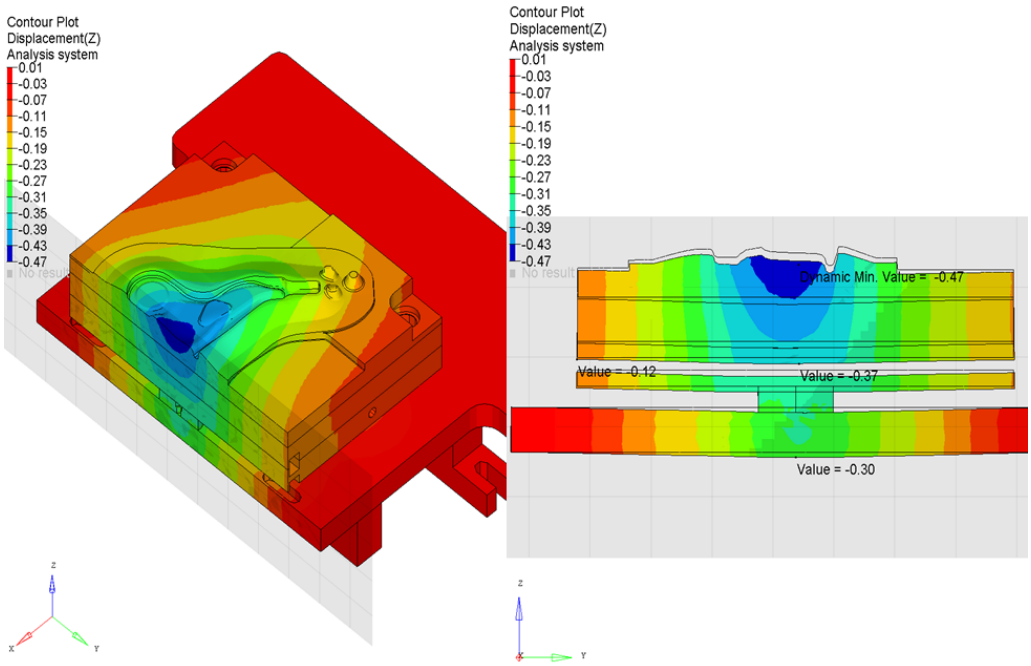

Figure 53: Lower tool nodal displacement (Z-direction). Min value = -0.47mm

Figures 48 and 49 show the stress contours developed on the upper and lower forming tool, respectively. They remain well below the yield stress of the material; a maximum stress of 270 MPa was observed. A conservative approximation of 650 MPa yield stress at 400℃ was derived from the literature for untreated 4140 steel [42]. The highest stress was observed in one of the support pucks in the lower tool. Figures 50 and 51 show localized yielding of a support puck with a maximum stress of 842 MPa. The remaining pucks in both the upper and lower tool do not exhibit yielding. Based on these results, the use of heat treated 4140 steel pucks which would have a higher yield stress was advised. Figures 52 and 53 show cross sectional views of the tool taken from the centre of the tool length along the x-axis. The maximum deflection observed in the upper tool was 0.26 mm, and 0.47 mm in the lower tool. Based on these values, the dimensional deviations likely to occur in the component due to the elastic behavior of the tool are within acceptable limits (IT12-IT16 of ISO IT standards).

Chapter 5
Control Arm Performance Analyses

The performance of the final control arm geometry, 13097-0000-2 R009 was evaluated using the three complete material models which were available at the time. The material models were developed using the tensile and cyclic property data of extruded AZ80, AZ31B, and ZK60 I-beam specimens forged at 250℃. Confidence in analysis accuracy was measured by first generating strength, stiffness and fatigue results for the extruded-forged AZ80 control arm at 250°C. Ford engineering test procedures [43] were followed to model, analyze and report the strength, stiffness and fatigue analysis results. The results were then compared with those generated by Prsa for the 13097-0002 R006 control arm geometry using the same forging material and condition [9]. Final component geometry is shown in Figure 54.

After the FEA model setup was validated, peak strength and minimum fatigue life performance of the component as a function of the other two forging materials and condition were analyzed. Strength results are expressed as a percentage of Ford strength requirements, and fatigue results are given in terms of minimum fatigue life of the component. Numerical performance results were compared alongside the analytical material selection model or objective function developed by the fatigue task group.

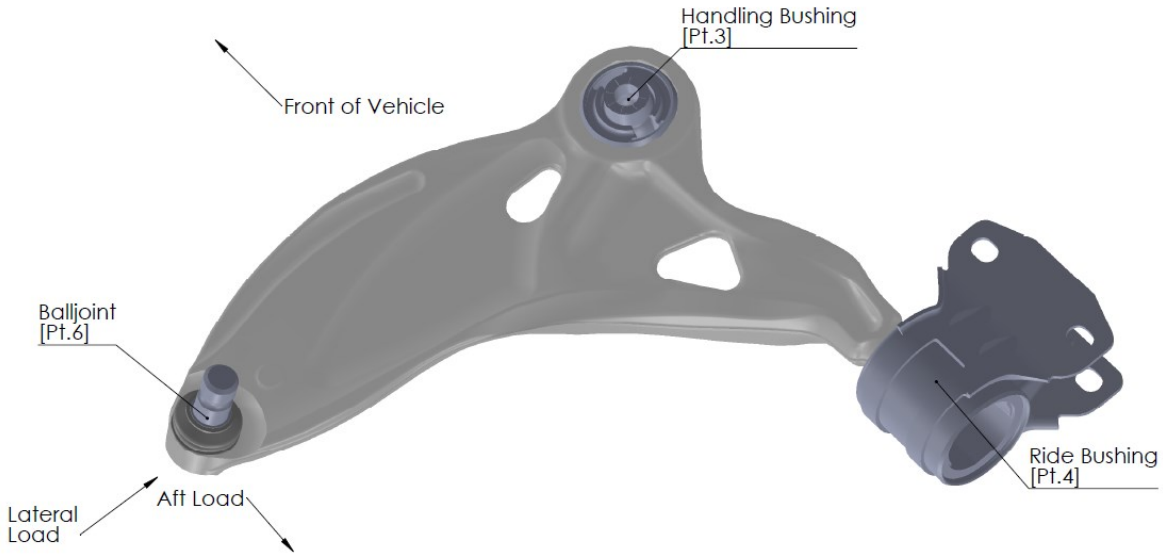

Figure 54: Final Control Arm Geometry

5.1.1 Finite Element Model

The finite element model of the final control arm was generated using HyperMesh 13.0. In order to mesh the component, the surface geometry was simplified and de-featured. The surface was meshed with a uniform second order M3D6 elements with a target size of 4 mm. This 2D mesh was then used to generate the interior 3D mesh with second order C3D10 tetra elements. Model information is provided in Table 9, and the control arm mesh is shown in Figure 55. Surfaces which would eventually be subjected to machining operations were separately distinguished for the purposes of assigning polishing and machining surface coefficients during fatigue analysis.

Table 9 : Model Information

	Element Type	Count
Surface Mesh (2D Membrane)	Abaqus M3D6	40240
Solid Mesh (3D)	Abaqus C3D10	139657

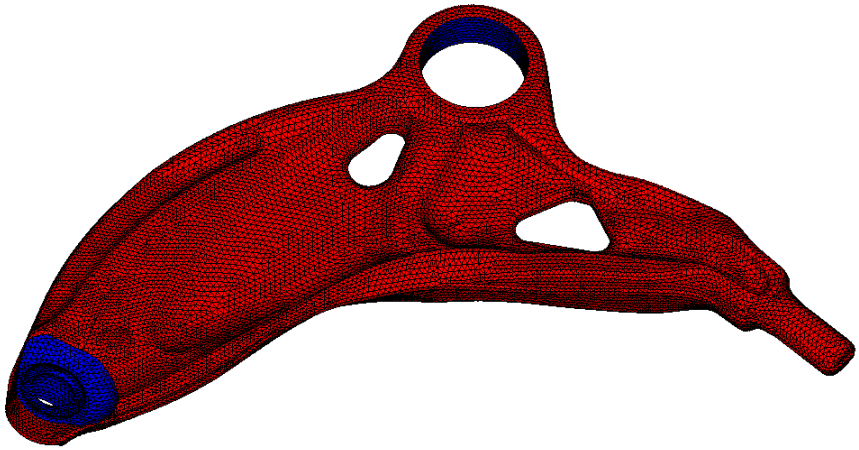

Figure 55: Control arm mesh. (Red) as-forged surface. (Blue) machined surface

Material stress-strain data for extruded AZ80 [44], AZ31B [44] , and ZK60 [33] forged at 250℃ are shown in Figure 56. The maximum plastic equivalent strain (PEEQmax) of each material is provided in Table 4.

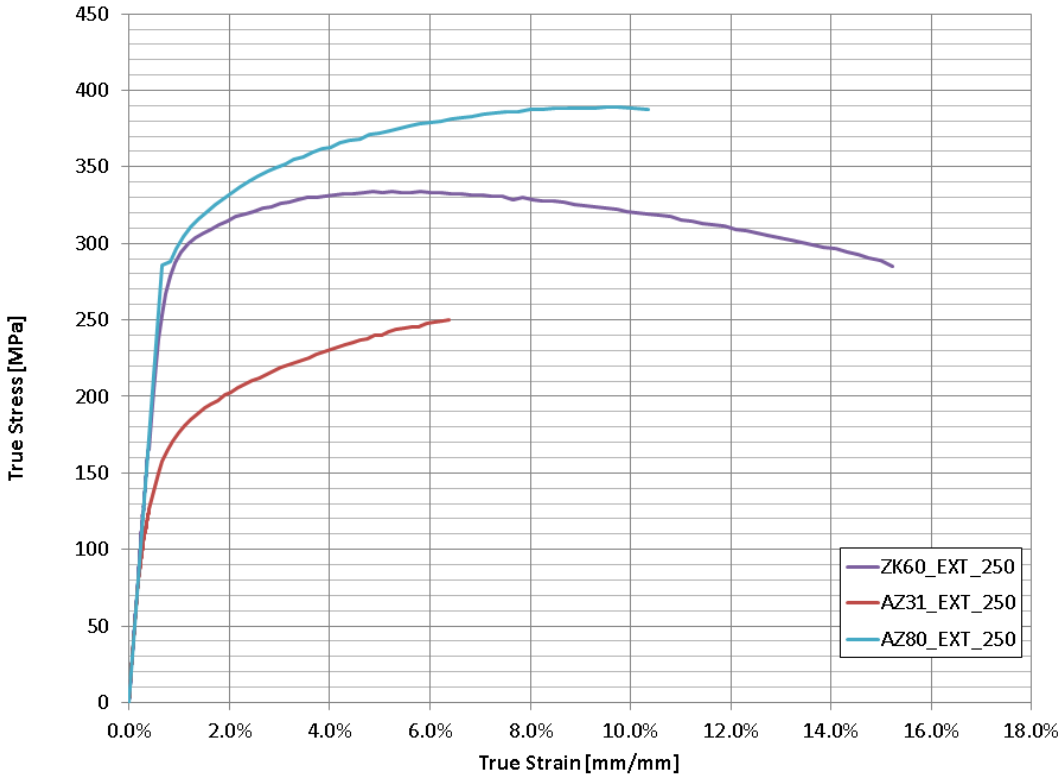

Figure 56: Comparison of Magnesium Material Models [45] [46] [44]

Table 10: Equivalent plastic strain of material (reproduced from [6])

Material	$PEEQ_{max}$ Allowable [%]
AZ31B Forged Magnesium	6
AZ80 Forged Magnesium	7
ZK60 Forged Magnesium	7

5.1.2 Finite Element Model Setup Validation

In order to validate the FEA model setup, structural and fatigue performance results of the final control arm, version 13097-0000-2 R009 was compared to the performance results generated by Prsa on 13097-0002 R006 version of the control arm. Geometrical differences between the two designs are shown in Figure 57; the balljoint region of the final control arm was modified and datum features for post-forging machining operations were added. Simulations were carried out using the same material property data for extruded AZ80 forged at 250℃. Structural performance was evaluated by conducting strength and stiffness analyses using Abaqus 6.13 solver. The finite element model was set up in accordance with Ford engineering test procedures [43]. The meshed component is connected directly to a simplified stiffness model of the suspension at hard points, balljoint (Pt. 6), hydro-bushing (Pt. 3), and ride bushing (Pt. 4) using RBE3 elements (refer to Figure 54). The suspension model, which was provided by Ford, was fixed at locations where the subframe mounts to the primary structure of the chassis. Simulations were performed using a global-level model in order to obtain more realistic deflections and load directions during analysis. The global-level model is shown in Figure 59.

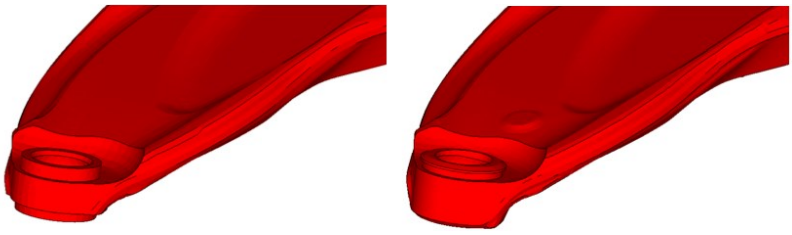

Figure 57: Geometrical differences between control arm designs. (Left) 13097-0002 R006. (Right) 13097-0000-2 R009.

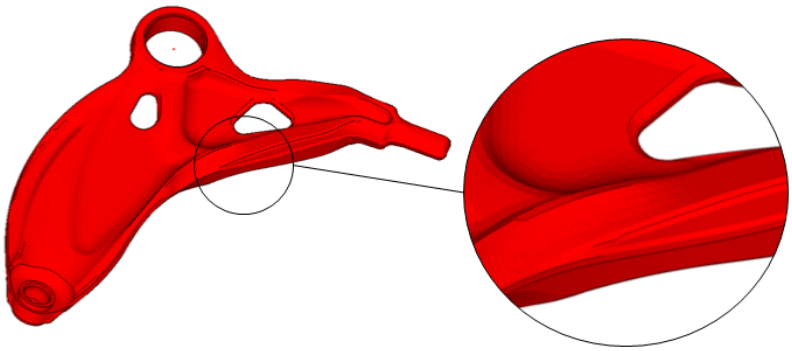

Figure 58: Tie-rod cut out region

The strength of the component was measured by subjecting it to a light overloading condition (L1 loads) representing loading which may occur over the course of component life, causing minimal deformation, and a heavier overloading condition (L2 loads) in which significant deformation, but not failure, is to be expected. Corresponding L1 and L2 loads were applied in the lateral and aft loading directions (refer to Figure 54). Component stiffness was evaluated by measuring deflection in the two directions. Finally, a fatigue analysis was conducted using nCode DesignLife v11.0 to determine the minimum life of the component. Author's results are compared to Prsa's results and expressed in the form of a percentage difference as shown in Table 9.

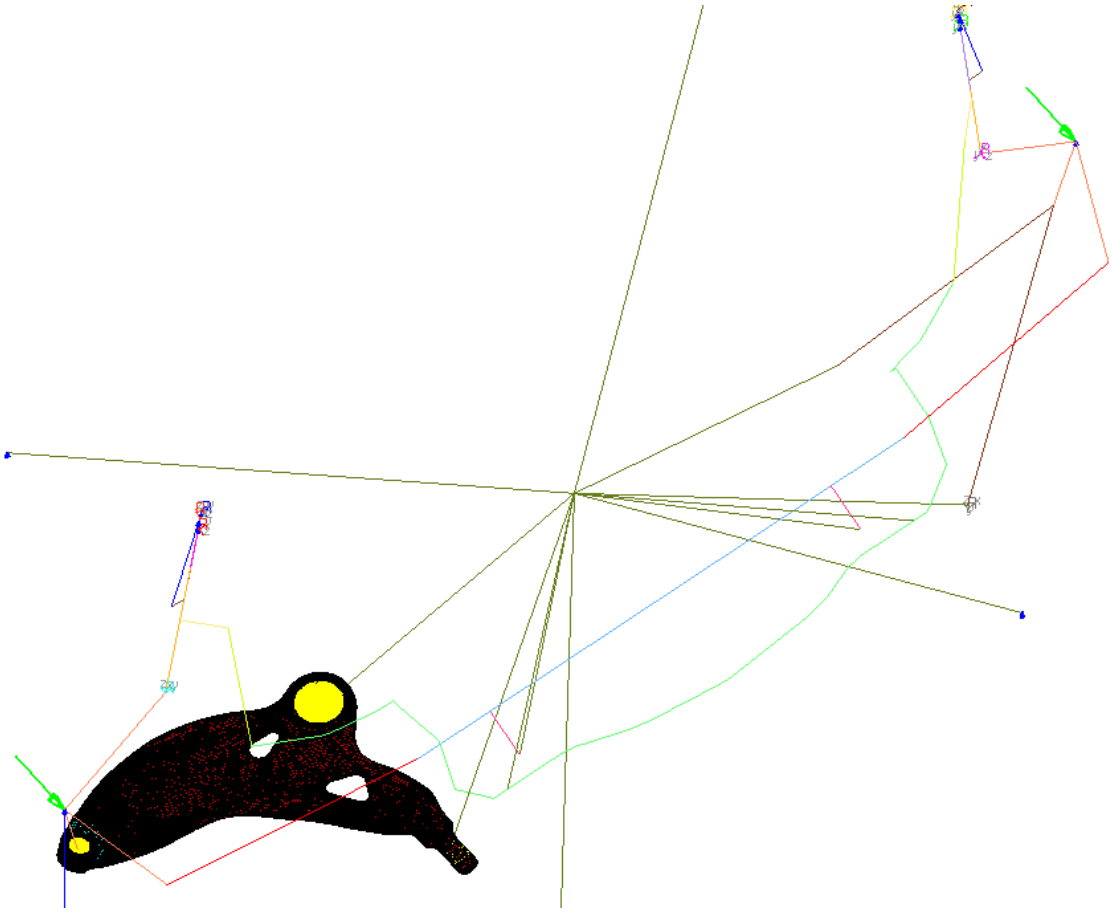

Figure 59: Global-level model. Control arm connected to suspension stiffness model

Table 11: Percentage difference between Author's and Prsa's control arm simulation results (Adapted from [9])

System-Level-Strength Analysis Results								Fatigue Life
Stiffness (RBE3)		L1 Aft		Peak Strain at L2 Aft Load	L1 Lateral		Peak Strain at L2 Lateral Load	
Aft [kN/mm]	Lateral [kN/mm]	Permanent Set [mm]	PEEQ Max [%]	P1 (Major) [%]	Permanent Set [mm]	PEEQ Max [%]	P1 (Major) [%]	[Lives]
1.4%	0.5%	+14.3%	0.0%	+17.4%	0.0%	0.0%	1.0%	-47.9%

L1 Aft permanent set and L2 Aft load peak strain results are 14.3% and 17.4% greater in comparison to Prsa's results, respectively. Permanent set and L2 peak strains in both models occur near the tie-rod cut out region (refer to Figure 58). The geometry in this region is unchanged between the two versions of the FLCA. Discrepancy between results may have arisen due the differences in the mesh, and or as a result of the version of Abaqus solver which was used [9]. The lowest fatigue life was measured near the tie-rod cut out region by author and near the balljoint region by Prsa; this region was modified in the final version of control arm design. Therefore, fatigue life near tie-rod cut out region in Prsa's simulation was used for comparison. The simulation performed by the author showed a decrease of fatigue life by 47.9% near this region in comparison to Prsa's simulation. This discrepancy can be attributed to the fact there is a noticeable change in geometry between the two models, and to the fact that a fatigue life analysis procedure is a logarithmic process, and a 10% error in loading magnitude could result in a 100% error in the predicted fatigue life [47].

5.1.3 Strength Analysis Results

Once the FEA model setup of the strength analysis was validated, the peak strain at L2 Aft loading – strength evaluation criteria was selected to measure the structural performance of the component as it captures the maximum strain of the component under load. To simulate component behaviour under this type of loading condition, the control arm load history was divided into three steps. First, the response of the skeleton model under static equilibrium was obtained. Then, the control arm was loaded with the gross vehicle weight. In the final step, the L2 load in the Aft direction was applied at the wheel center, and ramped up by the non-linear solver until the component was fully loaded or until component failure.

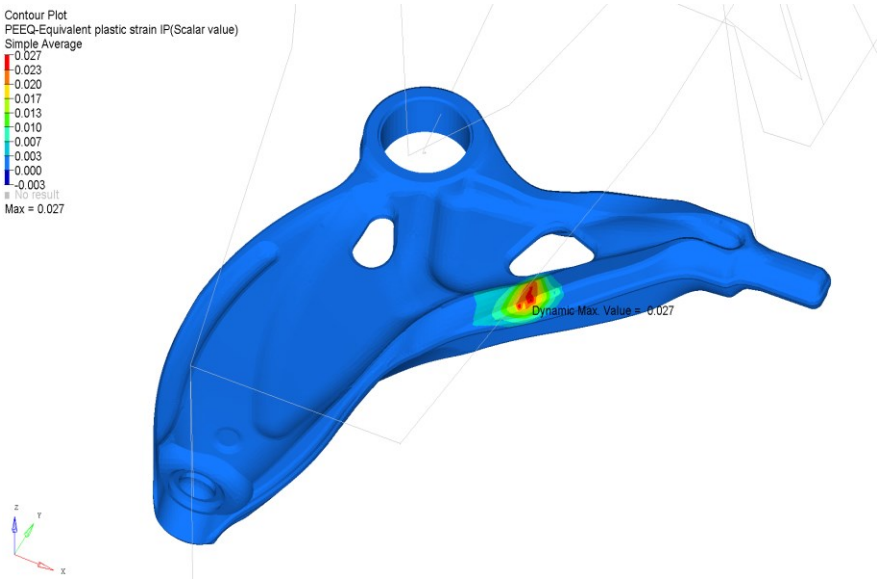

Figure 60: Deformed component forged using AZ80 alloy at 250℃. Achieved 100% of L2 load. Component experiences a maximum strain of 2.7%.

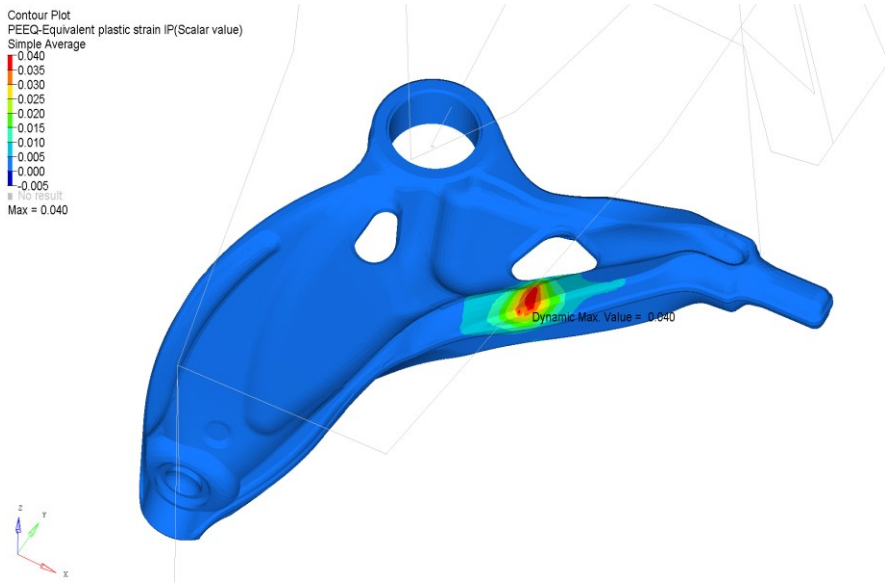

Figure 61: Deformed component forged using AZ31B alloy at 250℃. Achieved 66% of L2 load. Component experiences a maximum strain of 4.0%.

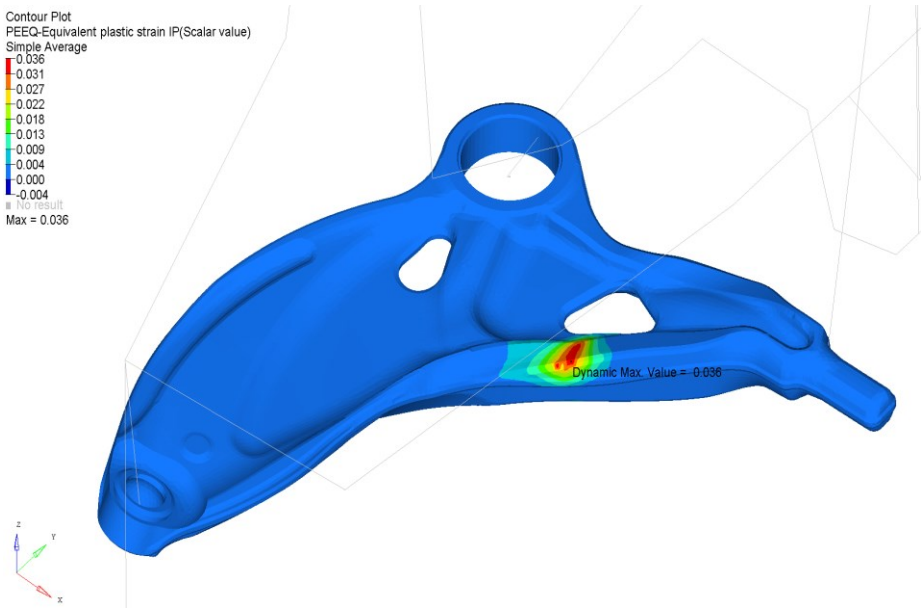

Figure 62: Deformed component forged using ZK60 alloy at 250℃ Achieved 97% of L2 load. Component experiences a maximum strain of 3.6%.

Contour plots of equivalent plastic strain are shown in Figures 60 to 62. During aft loading, significant amount of plastic strain develops over the rib region and tie-rod cut out for all three materials. Only the component assigned AZ80 extruded-forged at 250℃ material properties achieved a 100% load bearing capacity without failure, under L2 loading conditions. PEEQ strains remained below the allowable $PEEQ_{max}$ strains for all three materials. A full result summery is provided in Table 12. Control arms forged using different alloys at alternate temperatures may meet OEM strength specifications, if subjected to heat treatment processes after the forging operation.

5.1.4 Fatigue Life Analysis Results

The service life of the control arm was determined by conducting a fatigue life analysis of the control arm under a set of OEM-specified fatigue load cases. These results could not be validated with Prsa's fatigue analysis model since loading effects are magnified in a fatigue analysis; loading effects are not the same in 13097-0002 R006 and 13097-0000-2 R009 versions of the control arm. Details of the analysis procedure can be found in Strong's thesis [6]and Ford engineering test procedures [43]. These load cases are represented in the form of simplified load histories, which are translated into component stress and strain histories. Initially, the component was subjected to a unit load analysis for all possible load application directions. Next, the load histories were superimposed with the stress distribution results from the unit load case analyses to obtain component stress and strain histories using nCode DesignLife. Fatigue damage of the control arm was calculated using a Coffin-Manson strain life curve [6]. A Neuber elastic plastic correction factor and Smith-Watson-Topper mean stress correction were used in the fatigue model [6]. Surface correction factors were applied to model the roughness of the forged and machined surfaces [9].

As shown in Figures 63 to 65, the minimum fatigue life in all three models occur in tie-rod cut out region; regions of low fatigue life appear near regions of high stress concentration. The minimum predicted fatigue life for the AZ80 and ZK60 control arms comfortably exceeds the OEM specifications, while the AZ31 control arm results are marginal. A full result summery is provided in Table 12.

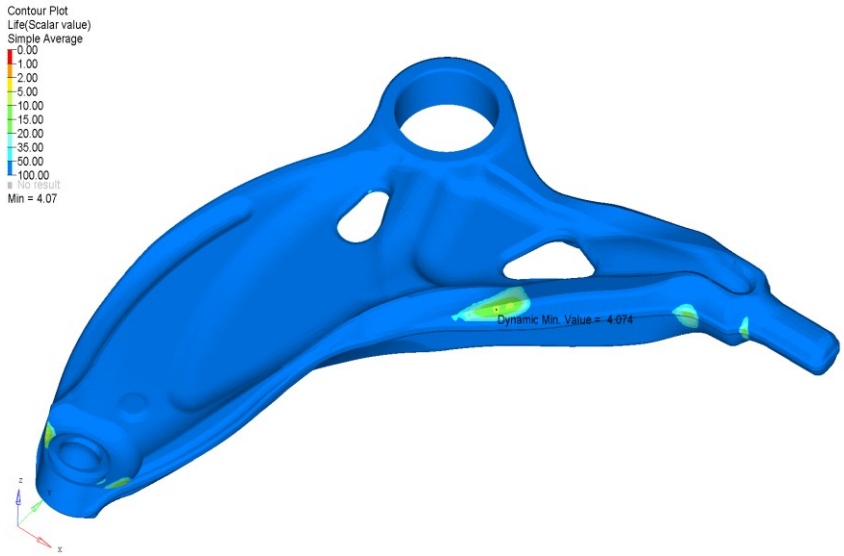

Figure 63: Minimum fatigue life of FLCA forged from AZ80 alloy at 250°C. Minimum fatigue life of the component is 4.07

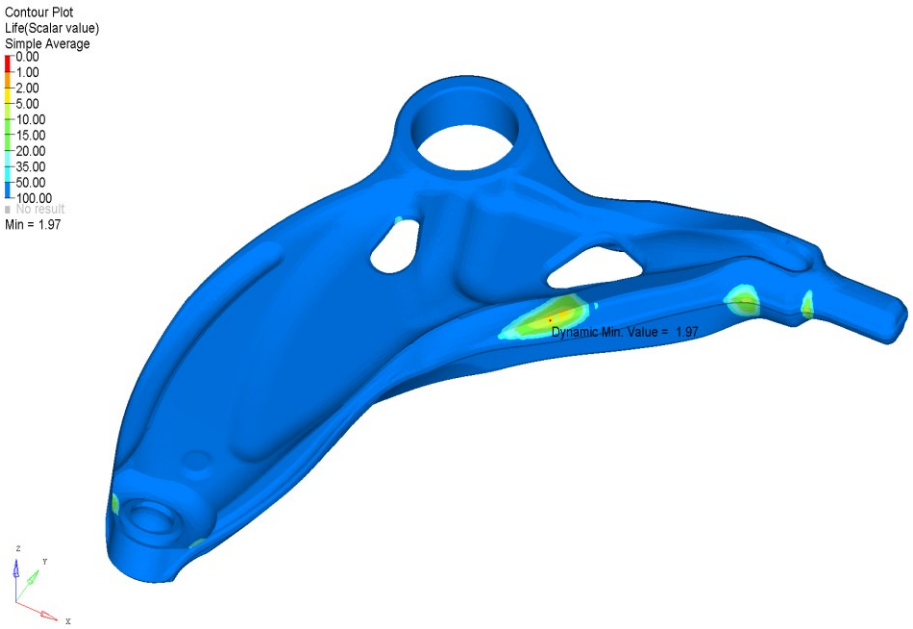

Figure 64: Minimum fatigue life of FLCA forged from AZ31B alloy at 250°C. Minimum fatigue life of the component is 1.97

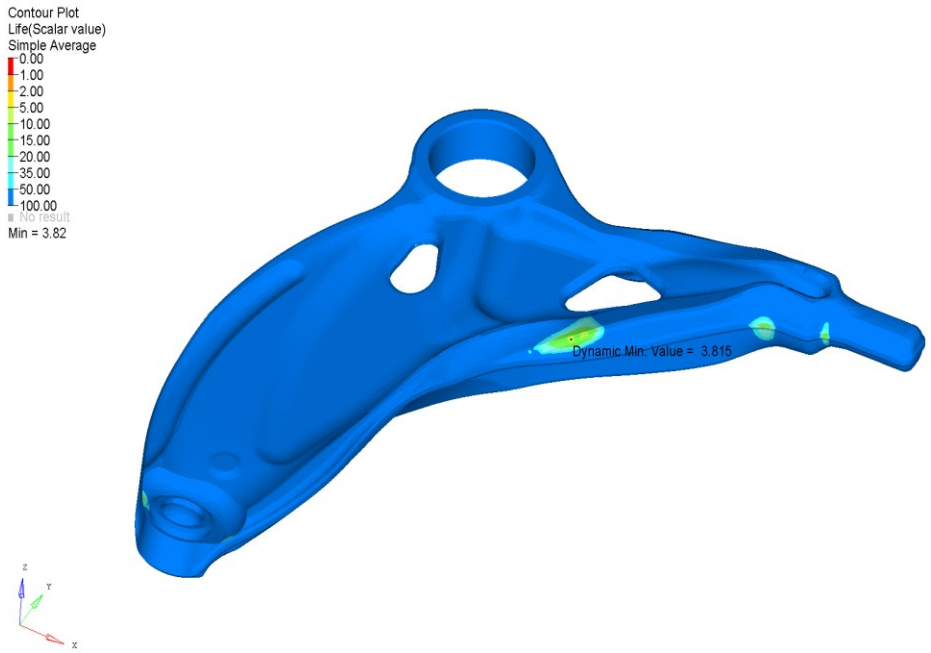

Figure 65: Minimum fatigue life of FLCA forged from ZK60 alloy at 250°C. Minimum fatigue life of the component is 3.81

Table 12: Tabulated strength and fatigue analysis results. Objective function score, φ, provided for each material forging condition

Alloy	Temperature °C	φ	Achieved [%] of L2	Fatigue life
AZ31 Cast + Forged	275	0.509	-	-
	375	0.511	-	-
AZ31 Extruded + Forged	250	0.698	66*	1.97
	375	0.72	-	-
ZK60 Cast + Forged	250	0.623	-	-
	375	0.566	-	-
ZK60 Extruded + Forged	250	0.814	96*	3.82
	375	0.745	-	-
AZ80 Cast + Forged	250	0.546	-	-
	275	0.466	-	-
	375	0.506	-	-
AZ80 Extruded + Forged	250	0.843	100	4.07
	375	0.739	-	-

[*] Indicates failed performance criteria

Table 12 shows the scores of the forged material derived from simulation, alongside forged material fitness scores derived using the objective function. Component strength was measured under L2 Aft loading – strength evaluation criteria, and was assigned the percentage of peak L2-Aft load sustained before failure or analysis completion; components capable sustaining L2-Aft loads or greater without failure are assigned an evaluation score of 100%. The minimum fatigue life values are directly recorded. Numerical analyses of the control arm performance conducted using the three material models yield insufficient information to make any direct claims about the effectiveness of the analytical material selection model due to two reasons: complete material models are needed for all forging conditions in order to simulate component performance to identify any correlations between the numerical and analytical results, and due to the that the fatigue analysis setup needs to validated.

Chapter 6
Conclusions and Recommendations

The scope of this research was the design and verification of a tool capable of hot forging a magnesium alloy control arm. Within this scope, a secondary task was carried out to evaluate the control arm performance using material properties of three forged magnesium alloys. Control arm performance results subject to each of the three alloys were used to examine the predictive accuracy of an analytical function developed by the Fatigue Task group to rank magnesium alloys and forging conditions.

6.1 Conclusions

The tool development process involved the identification of functional requirements and constraints. Factors such as component geometry, forging material, equipment, temperature, maximum tool load and the quantity of parts expected to be forged were identified. Based on these requirements and resources that were available at CanmetMATERIALS, a hot forging tool capable of forming a near-complete control arm with flash, in a single-hit operation, was designed and manufactured. The tool consists of an upper and lower forming tool, each internally heated with three 2500W Omegalux CIR-5142/240V electric heater cartridges. Cogetherm-M laminate insulation packages surrounding the tool to reduce heat transfer to the surrounding environment; it was critical that the forming surface temperature remain as uniform as possible during the forging process in order to minimize uneven thermal shrinkage of the forged component during cooling. Independent control of each internal heater cartridge is required to minimize the temperature gradient over the forming surface. Three Omega, BT-090-K-8-60-2 thermocouples were embedded in both the upper and lower forming tools to monitor the temperature of the forming surface. Material flow simulations were produced by Paracha [10]. Based on these simulations, modification to the upper and lower forming tools were made to minimize forging loads and ensure complete die filling. Once a suitable die design was developed, thermal and mechanical simulations were conducted to validate the tool. Simulation results revealed that by independently controlling the activation times of the heater cartridges, the temperature filed over the lower forming tool may be brought within a range of 370℃ and 400℃, and the upper tool, between 385℃ and 415℃. Mechanical performance was evaluated by subjecting a low-fidelity model of the tool to a maximum press load of 1600 tonnes. The load was applied as a uniform pressure over the preform and tool contact surface. Results from this simulation indicated that the stresses developed in the upper and lower forming

tools remain well below the 650 MPa yield stress of the material; a maximum stress of 270 MPa was observed in the lower forming tool. However, a support puck in the lower tool showed signs of yielding, suggesting the need to heat-treat the pucks to increase their strength; a maximum stress of 832MPa was observed in the puck.

Finite element simulations of the magnesium control arm performance indicate a successful component design capable of achieving the structural design requirements established by the OEM, when forged with an extruded AZ80 alloy at 250℃. The component geometry would need to be further optimized if it were to be forged using AZ31B and ZK60 alloys at 250℃; simulation results indicated component failure under heavy, L2 loading conditions. The control arm performance results were used to rank the three alloys which were then compared with the rankings assigned using the analytical function; both sets of data agreed with one another.

6.2 Recommendations

Recommendations which may be beneficial for future work in hot forging magnesium alloys are grouped according to topics covered in the document.

Tool Design

1. Contact pressures on the forming tool during peak loads of the forging cycle should be captured during DEFORM 3D simulations. These pressure profiles should then be superimposed on a high fidelity tool model including fasters, pad retainers and insulation laminates, to be solved to obtain the best estimates of the mechanical stresses and deflections in the tool. Stiffness in the press bed should also be taken into account. This would provide more a more accurate picture of the dimensional errors caused by tool heating, elasticity of the press, and the tooling system. A simulation capturing this level of detail is recommended for developing a single or a multi-stage processes for high volume production.

2. A wear analysis should be performed in order to ready the forging tool for high volume production. The analysis should take into account sliding velocity, operational temperature, contact time and accurate contact pressures at the contact interface of the work-piece and forming

tool in order to accurately predict the mechanical wear in the tool. The contact pressures can be obtained from DEFORM 3D forging simulations.

3. Heater cartridge distance in relation to the forming surface and one another should be optimized with the aim of achieving a more uniform duty cycle for all six cartridges, while minimizing the temperature gradient over the forming surface. It may be better overall to eliminate a separate heating plate, and redesign the forming tool with bore holes for heater cartridges. Also, a tool designed for high volume production rates needs to account for thermal disturbances caused by opening and closing the upper and lower tools as each successive forming operation will cause the tool temperature to gradually change. Additional heat gains and losses during continuous operation would need to be determined.

Control Arm Geometry Optimization

1. Numerical analyses should be carried out using all material forging conditions in order to compare performance scores with the analytical scores assigned using the objective function. Correlations between component geometry and material forging conditions may become observable when component performance is simulated using all 13 material models.

2. The current geometry of the control arm is obtained for an extruded AZ80 material, forged at 250℃. Control arms that are forged using a different Mg alloys at varying forging conditions, as shown in Chapter 5, are incapable of meeting OEM specifications. Therefore, if alternate alloys were to be used, or the control arm were to be forged at different temperatures, it would be necessary to further modify the geometry of the control arm. It is necessary to simulate the performance of the current FLCA geometry using the remaining materials and forging conditions in order to identify regions of undesired stress concentrations. Once these regions have been identified, a shape optimization can be performed to produce an optimized component geometry capable of meeting the OEM requirements.

References

[1] H. Jahed, "Optimum Design of Fatigue-Critical Automotive Components Made of Magnesium Alloys," 2013.

[2] L. Cheah, C. Evans, A. Bandivadekar and J. Heywood, "Factor of Two: Halving the Fuel Consumption of New US Automobiles by 2035," MIT Laboratory for Energy and Environment, Cambridge, MA, 2007.

[3] M. M. Avedesian and H. Baker, "ASM Specialty Handbook," in *Magnesium and Magnesium Alloys*, 1999, p. 3–6.

[4] T. Byrer, S. Semiatin and D. Vollmer, Forging Handbook, Ohio: Forging Industry Association , 1985.

[5] S. Fleming, "An Overview of Magnesium based Alloys for Aerospace and Automotive Applications," Rensselaer Polytechnic Institute, Hartford, CT, 2012.

[6] A. Strong, "Optimization of Forged Magnesium Structural Automotive Components," 2016. [Online]. Available: UWSpace. http://hdl.handle.net/10012/10692.

[7] G. Yu, "Forging specimen design for Mg alloys," 2016. [Online]. Available: UWSpace. http://hdl.handle.net/10012/10690.

[8] O. Udarchik, Interviewee, *Design Engineer, Multimatic Technical Centre.* [Interview]. 2017.

[9] J. Prsa, Interviewee, *Lead Structures Engineer, Multimatic Technical Centre.* [Interview]. 2017.

[10] T. Paracha, "Modelling of the Forging Process for a Magnesium Alloy Automotive Control Arm," 2018. [Online]. Available: UWSpace. http://hdl.handle.net/10012/13216.

[11] T. Altan and M. Shirgaokar, "Process Design in Impression Die Forging," in *Cold and Hot Forging Fundamentals and Applications*, Ohio , ERC/NSM, NSM Laboratory, Ohio State University, 2005, pp. 159-181.

[12] J. Langner, M. Stonis and B.-A. Behrens, "Investigation of a moveable flash gap in hot forging," *Journal of Materials Processing Technology,* vol. 231, pp. 199-208, 2106.

[13] R. H. Wagner and J. Chenot, Fundamentals of Metal Forming, Wiley, 1996.

[14] Stamping Journal, "R&D Update: Warm-forming magnesium sheet, Part I," thefabricator.com, 10 11 2017. [Online]. Available: https://www.thefabricator.com/article/stamping/die-science-warm-forming-magnesium-sheet-part-i. [Accessed 26 08 2018].

[15] P. Skubisz, J. Sinczak and S. Bednarek, "Forgeability of Mg–Al–Zn magnesium alloys," *Material Processing Technology ,* vol. 177, pp. 210-213, 2006.

[16] T. Altan, F. W. Boulger, J. R. Becker, N. Akgerman and H. J. Henning, "Forging Equipment, Materials and Practices," Batelle Columbus Laboratories Metalworking Division, Ohio, 1973.

[17] J. McKinley, Interviewee, *Solid Metal Processing Engineer, CanmetMATERIALS.* [Interview]. 18 January 2018.

[18] J. Cermak and G. Graf, "Die Design for Near-Net Shape Forging," *Acta Polytechnica,* vol. 43, pp. 28-33, 2003.

[19] A. Gryguc, S. K. Shaha, S. B. Behravesh, H. Jahed, M. Wells, B. Williams and &. X. Su, "Monotonic and cyclic behaviour of cast and cast-forged AZ80 Mg," *International Journal of Fatigue,* vol. 104, p. 136–149, 2017.

[20] D. Toscano, "Characterization of the Quasi-Static and Fatigue Behavior of Forged AZ31B Magnesium Alloy," 2018. [Online]. Available: https://uwspace.uwaterloo.ca/bitstream/handle/10012/13095/Toscano_Dwayne.pdf?sequence=7&isAllowed=y.

[21] M. Terelj, I. Perus and R. Turk, "Suitability of CAE Networks and FEM for Prediction of Wear on Die Radii in Hot Forging," *Tribology International,* vol. 36, pp. 573-583, 2003.

[22] J. Kang, I. Park, J. Jae and S. Kang, "A study on a die wear model considering thermal softening (I): construction of the wear model," *J. Mater. Process. Technol.,* vol. 96, pp. 53-58, 1999).

[23] R. Douglas and B. Kuhlmann, "Guidelines for precision hot forging with applications," *Journal of Material Process Technology ,* no. 98, pp. 182-188, 2000.

[24] N. Joseph, "Investigation of Surface Roughness and Lay on Metal Flow in Hot Forging," Master's Thesis (2009).

[25] F. I. Association, "Design Rules For Parts Made From Impression Die," 05 03 2017. [Online]. Available: https://www.forging.org/forging/design/3541-design-rules-parts-made-impression-die-forgings.html.

[26] O. S. University, "Forging Process Design," 2015. [Online]. Available: https://ercnsm.osu.edu/sites/ercnsm.osu.edu/files/uploads/F-hotforging/467.pdf. [Accessed 31 10 2016].

[27] A. Hedrick, "Die basics 101 starts with eight basic components," The Fabricator, 08 08 2006. [Online]. Available: https://www.thefabricator.com/article/stamping/die-basics-101-starts-with--eight-basic-components. [Accessed 05 04 2017].

[28] T. A. D. Company, "Anchor Danly," [Online]. Available: http://www.anchordanly.com/PDFs/AnchorDieSets.pdf. [Accessed 05 04 2017].

[29] P.C.Sharma, A Textbook of Production Engineering, Ram Nagar: S.Chand & Company ltd. , 1999.

[30] MHI, Writer, *Simulation of die heating for forgings and pressure castings by convective heating systems.* [Performance]. Airtorch™, 2018.

[31] Instrumart, "Application Guide," [Online]. Available: https://www.instrumart.com/assets/heater_application_guide.pdf. [Accessed 26 08 2018].

[32] A. S. f. Metals, Metals Handbook – Forging and Casting, Ohio: ASM Handbook Committee, 1971.

[33] R. Hill, "A theory of the yielding and plastic flow of anisotropic metals," *Proceedings of The Royal Society of London. London: The Royal Society,* pp. 281-297, 1948.

[34] H. Zwaan, Interviewee, *Tool Maker, Multimatic Technical Centre.* [Interview]. 2018.

[35] O. Engineering, "High Watt Density Cartridge Heaters with Incoloy," Omega, [Online]. Available: https://www.omega.com/pptst/CIR_34.html. [Accessed 18 10 2017].

[36] D. Systems, "Abaqus Example Problems Guide, vol1," 2014. [Online]. Available: http://130.149.89.49:2080/v6.14/pdf_books/EXAMPLES_1.pdf. [Accessed 17 02 2018].

[37] R.L.Echavarria and J.V.Namjoshi, "Simulation of Residual Stresses in Castings," Tekniska högskolan, Stockholm, 2007.

[38] A.Al-Rifaie, Z. Guan and S.W.Jones, "Quasi-Static Analsyiss of End Plate Beam-to-Column Connections," *International Journal of Civic and Enviornmental Engineering,* vol. 11, no. 7, 2017.

[39] G. Camp and N.Drivakos, "FEM analysis of a gearbox housing, for the calculation fo stress and deflection characteristics," Volkswagen A.G., BETA CAE Systems S.A..

[40] M. Tannert, C.Brecher, S.Baumler and K.Bakarinow, "Modeling of Machine and Tool Elasticity in Coupled Forging Simulation," RWTH Aachen University , Aachen.

[41] P. Plastics, "Cogetherm® - Mica Laminate Insulation Board," [Online]. Available: https://www.professionalplastics.com/professionalplastics/CogethermDataSheet.pdf. [Accessed 03 09 2018].

[42] R.S.DeFries, "The Elevated Temperature properties of Two 81mm Mortar Tube Alloys 4337M and 4140," Benet R&E Labratories, New York, 1971.

[43] Ford, "Link arm Strength Analysis Procedure," Ford, 2011.

[44] A.Gryguc, Interviewee, *HQP, Fatigue Task Group.* [Interview]. 10 January 2018.

[45] D. Toscano, Interviewee, *HQP, Forging Task Group.* [Interview]. 15 January 2018.

[46] S. Karparvarfard, Interviewee, *HQP, Fatigue Task Group.* [Interview]. 08 January 2018.

[47] P. Marketing, "What is Fatigue Analysis?| MSC Nastran," MSC Software, 01 07 2013. [Online]. Available: http://simulatemore.mscsoftware.com/what-is-fatigue-analysis-msc-nastran/. [Accessed 09 04 2018].

[48] C. Szasz, "Air Gap Insulated Exhaust Manifold," 2011. [Online]. Available: https://diglib.tugraz.at/download.php?id=576a8d95a1889&location=browse.

[49] T. Bergman, A.S.Lavine, F. Incropera and D.P.Dewitt, Fundamentals of Heat and Mass Transfer, United States of America : John Wiley & Sons, 2011.

[50] M. Baxter, Product Design, Boca Raton: CRC Press, 1995.

[51] D. Nowak, "Investigation of Surface Roughness and Lay on Metal Flow in Hot Forging"," in *Marquette University*, Master's Thesis (2009) .

Appendix A
Analytical Calculations

Cartridge Power Calculations

The total energy required to raise the temperature of both the impression tool and heater block from room temperature to 350℃ of either the upper or lower forging tool assemblies is determined (impression tool and heater block pairs have similar weights):

Q_1 - Energy required to raise the temperature of material (Wh):

w - Weight of the impression die and heater block (lbs):

ΔT- Temperature rise in material ($T_{Final} - T_{initial}$)(°F)

$$Q_1 = \frac{w \cdot c_p \cdot \Delta T}{3.412}$$

$$Q_1 = \frac{1140\ lbs \cdot 0.11\ \frac{BTU}{lb - °\mathrm{F}} \cdot (662 - 70)°\mathrm{F}}{3.412}$$

$$Q_1 = 21831\ Wh$$

The energy required to maintain the forging tool temperature at 350℃ is determined by accounting for side wall and bottom surface heat loss through 1 inch thick insulation:

Q_2- Energy lost due to convection heat loss from side walls at 350℃ (w-h):

Q_3- Energy lost due to convection heat loss from bottom surface at 350℃ (w-h):

A - Surface area (in^2)

C_f - Surface orientation factor (vertical = 1.00)

F_{sl} - Vertical surface convection loss factor evaluated at surface temperature of a 1 in. thick insulation at surface temperature of 350 °C ($\frac{W}{in^2-h}$).

k - Thermal conductivity of insulation ($\frac{BTU \cdot in}{ft^{2.\circ}\text{F} \cdot h}$)

$$Q_2 = C_f \cdot F_{sl} \cdot A$$

$$Q_2 = 1.00 \cdot 0.7 \frac{W}{in^2 - h} \cdot 377\ in^2$$

$$Q_2 = 264\ Wh$$

$$Q_3 = \frac{k \cdot A \cdot \Delta T}{3.412 \cdot L \cdot h}$$

$$Q_3 = \frac{0.76 \frac{BTU \cdot in}{ft^2 \cdot °\text{F} \cdot h} \cdot 4.86 ft^2 \cdot (662 - 70)°\text{F}}{3.412 \cdot 1\ in \cdot h}$$

$$Q_3 = 640\ Wh$$

The total energy required to maintain the lower tool die and heater block at a uniform temperature of 662°F or 350°C:

$$Q_{Total} = Q_1 + Q_2 + Q_3$$

$$Q_{Total} = 2131\ Wh + 264\ Wh + 640\ Wh$$

$$Q_{Total} \approx 23.0\ kWh$$

The total energy required to raise and maintain the temperature of both the lower and upper forging tool assemblies, therefore would surmount to $46.0\ kWh$. Each forging tool assembly would consist of three heater cartridges. With the expectation that the tool heating time will be approximately 3.5 hours, the power output requirement from a single heater cartridge can be determined:

$$P_{heater\ cartridge} \approx 2500\ W$$

Support Puck Load Calculation Equations

$F_{max\_press\_load}$ − Maximum force applied on the puck surface by the press tool

A_{pucks} − Load bearing surface area of pucks

N − Number of pucks

$$P = \frac{F_{max\_press\_load}}{A_{pucks}}$$

$$\sigma_{yeild} = \frac{F_{max\_press\_load}}{N(\pi \cdot r^2)}$$

$$r = \sqrt{\frac{F_{max\_press\_load}}{N \cdot \pi \cdot \sigma_{yeild}}}$$